Shape Recovery Algorithms Using Level Sets in 2-D/3-D Medical Imagery: A State-of-the-Art Review

Jasjit S. Suri, *Senior Member, IEEE*, Kecheng Liu, Sameer Singh, *Member, IEEE*, Swamy N. Laxminarayan, *Senior Member, IEEE*, Xiaolan Zeng, *Member, IEEE*, and Laura Reden

***Abstract*—The class of geometric deformable models, also known as level sets, has brought tremendous impact to medical imagery due to its capability of topology preservation and fast shape recovery. In an effort to facilitate a clear and full understanding of these powerful state-of-the-art applied mathematical tools, this paper is an attempt to explore these geometric methods, their implementations and integration of regularizers to improve the robustness of these topologically independent propagating curves/surfaces. This paper first presents the origination of level sets, followed by the taxonomy of level sets. We then derive the fundamental equation of curve/surface evolution and zero-level curves/surfaces. The paper then focuses on the first core class of level sets, known as "level sets without regularizers." This class presents five prototypes: gradient, edge, area-minimization, curvature-dependent and application driven. The next section is devoted to second core class of level sets, known as "level sets with regularizers." In this class, we present four kinds: clustering-based, Bayesian bidirectional classifier-based, shape-based and coupled constrained-based. An entire section is dedicated to optimization and quantification techniques for shape recovery when used in the level set framework. Finally, the paper concludes with 22 general merits and four demerits on level sets and the future of level sets in medical image segmentation. We present applications of level sets to complex shapes like the human cortex acquired via MRI for neurological image analysis.**

***Index Terms*—Cortex, deformable models, differential geometry, front, fuzzy, level sets, propagation, regularization, segmentation, stopping forces, topology.**

I. Introduction

THE ROLE of shape recovery has always been a critical component in two-dimensional (2-D) and three-dimensional (3-D) medical imagery since it assists largely in medical therapy (see the recent book by Suri *et al.* [1] and references therein). The applications of shape recovery have been increasing since scanning methods became faster, more accurate and less artifacted (see [1, Ch. 4] or [2]). The recovery of shapes of the human body is more difficult compared to other imaging fields. This is primarily due to the large variability in shapes, complexity of medical structures, several kinds of artifacts and restrictive[1] body scanning methods. In spite of the above-mentioned complications, an exploration has begun into obtaining faster and more accurate software tools for shape recovery in 2-D and 3-D. This paper is an attempt to survey the latest techniques in 2-D and 3-D for fast shape recovery based on the class of deformable models, known as "level sets" or "geodesic active contours/surfaces."[2]

The application of the level sets in medical image segmentation became extremely popular because of its ability to capture the topology of shapes in medical imagery. Recently, Lachaud (see [4]–[6]) and Malgouyres *et al.* [7] showed a relationship between topology and isosurface extraction. Malgouyres *et al.* [7] also recently published an excellent paper on topology preservation within digital surfaces. A detailed survey on digital topology in computer vision, graphics, and image processing (CVGIP) can be seen by Kong *et al.* [8] and also the related research work by Bertalmio *et al.* [9] and DeCarlo *et al.* [10]. The diversity of applications of level sets has reached into several fields. These applications and their relevant references are listed here: 1) geometry: (see Angenent *et al.* [11], Chopp *et al.* [12], [13] and Sethian *et al.* [14]); 2) grid generation: (see Sethian *et al.* [15]); 3) fluid mechanics: (see Mulder *et al.* [16], Sethian *et al.* [17] and Sussman *et al.* [18]); 4) combustion: (see Rhee *et al.* [19]); 5) solidification: (see Sethian *et al.* [20]); 6) device fabrication: (see Adalsteinsson *et al.* [21]); 7) morphing: (see Whitaker *et al.* [22]–[24]); 8) object tracking/image sequence analysis in images: (see the recent work by Mansouri *et al.* [25]–[27], Paragios *et al.* [28], [29] and Kornprobst *et al.* [30]); 9) stereo vision: (see the recent work by Faugeras and his coworkers at INRIA [31]); 10) shape from shading: (see Kimmel *et al.* [32]–[34]); 11) mathematical morphology: (see Arehart *et al.* [35], Catte *et al.* [36], Sapiro *et al.* [37] and Sochen *et al.* [38]); 12) color image segmentation: (see Sapiro *et al.* [39]); 13) 3-D reconstruction and modeling: (see Caselles *et al.* [40] and [41]); 14) surfaces and level sets: (see Chopp *et al.* [42] and Kimmel *et al.* [43]); 15) topological evaluations: (see DeCarlo *et al.* [10]); and 16) 2-D and 3-D medical image segmentation: (see these works by Malladi *et al.* [44]–[48], [50], [49], Yezzi *et al.* [51]); gray matter/white matter (GM/WM) boundary estimation by Gomes *et al.* [52]; GM/WM boundary estimation with fuzzy models by Suri *et al.* [53]; GM/WM thickness estimation by Zeng *et al.* [54]; leaking prevention in fast level sets by Suri *et al.* [55]; a recent survey article on brain segmentation by Suri *et al.*

Manuscript received October 3, 2000; revised January 29, 2001 and April 3, 2001.

J. S. Suri, K. Liu, and L. Reden are with the MR Clinical Science Division, Philips Medical Systems, Inc., Cleveland, OH 44143 USA.

S. Singh is with PANN, Department of Computer Science, University of Exeter, Exeter EX4 4PT U.K.

S. N. Laxminarayan is with the Department of Biomedical Engineering, New Jersey Institute of Technology, Newark, NJ 07102 USA.

X. Zeng is with R2 Technology, Inc., Los Altos, CA 94022 USA.

Publisher Item Identifier S 1089-7771(02)00028-6.

[1]Scanning ability limited to acquiring in three orthogonal and oblique directions only.

[2]We will interchangably use the phrase "level sets" and "geodesic active contour/surfaces."

[57]; application of level sets for cortex unfolding by Faugeras and his coworkers from INRIA (see Hermosillo *et al.* [58]); application of the level set technique in cell segmentation (see Sarti *et al.* [59]); and Niessen *et al.* [60] for the application of geodesic active contours for cardiac image analysis. For a detailed review of some of these above applications, readers must see the works by Sethian *et al.* [61], [62] published in 1989 and 1996, respectively, and Kimmel *et al.* [63]. Though these survey publications cover a good collection of level set applications, with the advancement of image processing technology, these publications fall behind in: 1) the latest trends, the so-called design of the robust propagation forces, which is the crux of this paper; and 2) not having a proper focus on the medical imaging area. Both these shortcomings will be removed in this paper. Having discussed the importance and application of level sets, the paper now presents the place of level sets in the segmentation tree and its taxonomy.

The taxonomy of level sets for segmentation of 2-D and 3-D medical imagery can be seen in Fig. 1 (top). (For details on segmentation techniques, readers are referred to exhaustive reviews by Suri *et al.* [64] and [57].) Fig. 1 (top) shows the classification of 2-D and 3-D segmentation techniques, divided into three core classes: 1) region-based; 2) boundary/surface-based; and 3) fusion of boundary/region-based. The second core class of segmentation is also known as "deformable models" and the third core class is also called the "fusion of regions with deformable models." The deformation process has played a critical role in shape representation. This paper uses "level sets" as its tool to capture deforming shapes in medical imagery. The research in deformation started in the late 1980s when the paper called "snakes" (the first class of deformable models) was published by Terzopoulous *et al.* [65] and Kass *et al.* [66]. Since then, there has been an extensive burst of publications in the area of parametric deformable models and their improvements, such as balloon force and template-based fitting (see all of these references in by Suri *et al.* [1, Ch. 3 and 4]). Discussions on these references are out of the scope of this paper. The second class of deformable models is level sets. These deformable models were started by Osher and Sethian [67], which started from Sethian's Ph.D. dissertation [68]. The fundamental difference between these two classes is: Parametric deformable curves (active contours) are local methods based on an energy-minimizing spline guided by external and image forces which pull or push the spline toward features such as lines and edges in the image. These classical active contour models solve the objective function to obtain the goal boundary, if the approximate or initial location of the contour is available. On the other hand, level set methods are active contour energy minimization techniques which solve computation of geodesics or minimal distance curves. Level set methods are governed by curvature dependent speeds of moving curves or fronts. Those familiar in the field of active-modeling will appreciate these major advantages and superiority of level sets compared to classical deformable models. These will be covered in this paper as well.

Geometric deformable models[3] or level set techniques are classified broadly into two classes (see Fig. 1, top, shown in dotted line area): 1) without regularizers; and 2) with regularizers. Level sets without regularizers are techniques where the propagation force does not utilize the region-based strategy for its computation. These forces are constant and do not change. Sometimes they are also called as "level sets stoppers." Earlier research called these "leakage prevention" techniques because they tried to prevent any bleeding of boundaries during propagation. These are further classified into five different kinds, depending upon the design of the stopping force: 1) gradient-based stopping force; 2) edge-based stopping force; 3) area-minimization-based stopping force; 4) curvature-based stopping force; and 5) application-driven level sets. The curvature-dependent class has four sub-classes: 1) plain curvature-based; 2) mean curvature flow based with directionality; 3) bubbles; and 4) morphing. Plain curvature based techniques are those which are driven solely by the curvature that is computed using differential geometry. Mean curvature flow with directionality-based techniques are those which use the combination of Euclidean curvature and direction together to achieve the deformation process. Such techniques are good for tiny, occluded, and twisted objects like blood vessels. Bubbles are a set of seeds, or fourth-order shocks, which grow, shrink, merge, split, disappear, and deform under the influence of image information such as edges and gradients to segment objects in images and volumes. Morphing techniques are those which undergo shape deformation from one initial shape to the target shape driven by the combination of signed distance at coordinate transformation and the gradient of the signed distance transform functions. This transformation captures the similarity between user-defined shape and target shape.

The second core class of level sets uses regularizers or level sets that derive the propagation force using statistical means such as region-based strategy. This is further classified into four types depending upon the design of propagation force. They are: 1) clustering-based; 2) classification based on Bayesian statistics; 3) shape-based; and 4) constrained coupled level sets where the propagation force is derived from Bayesian strategies.

Having defined the taxonomy of level sets in medical image segmentation, the following goals of this paper are presented: 1) To present the tentative taxonomy of level sets and its place in 2-D and 3-D medical image segmentation; 2) To understand the curve/surface propagation of hypersurfaces based on differential geometry; 3) To present the mathematical foundations of different techniques as discussed in the level set taxonomy [see Fig. 1 (top)]. This also includes a discussion of pros and cons of all techniques for curve/surface propagation; 4) To study different kinds of propagating forces[4] and their fusion in the level set formalism using partial differential equations (PDEs) for curve/surface propagation and evolution; 5) To present the state-of-the-art 2-D and 3-D level set segmentation systems for medical imagery along with their merits and demerits; and finally, 6) To present the state-of-the-art ready references for readers interested in further exploring into the field of medical imaging segmentation using level sets. Note that the goal of this paper is not to discuss the PDE-based image processing approaches, even though it is closely related (for details on

[3]We will interchangably use the word "geometric deformable models" or "level sets" or "geodesic contours" during the course of this paper.

[4]Also called as regularizers.

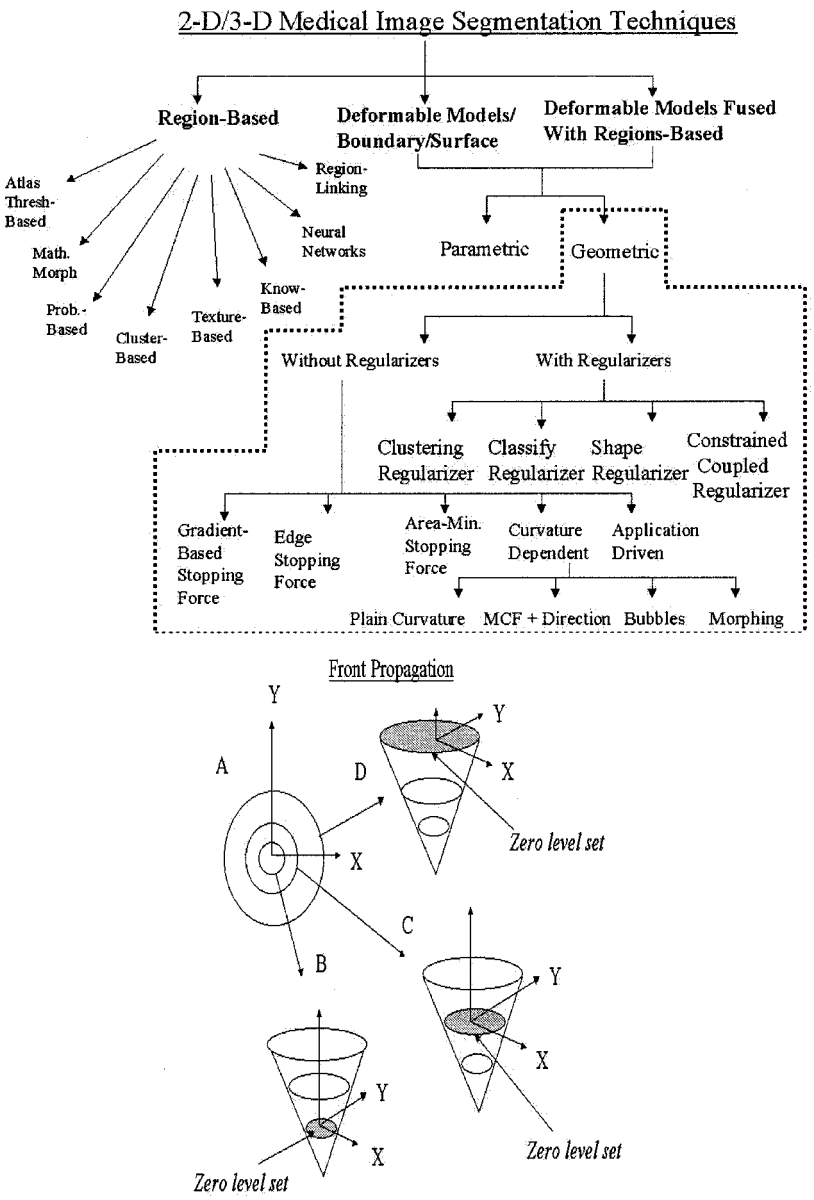

Fig. 1. Top: The place of level sets in the medical segmentation tree. Note the classification subtree of geometric deformable models or level sets (shown in dotted line area). Bottom: Front propagation of the *zero level set*. Filled circles in figures (B), (C), and (D) show the position of the *zero level curve* as the front propagates. These three projected circles are seen in figure (A).

PDE-based applications to image processing, see the upcoming paper by Suri *et al.* [69] and their references therein).

The layout of the remainder of this paper is as follows: Section II presents the introduction to level sets and the derivation of the curve evolution equation. Section III presents the first core class of level sets, i.e., "level sets without regularizers" and their subclasses. The second core class of level sets, i.e., "level sets fused with regularizers" for image segmentation, is discussed in Section IV. This is the crux of the paper and discusses the state-of-the-art method for design of the "propagating force" used for the deformation/morphing process in 2-D/3-D medical imagery. Section V covers numerical methodologies of level sets using finite differences. Optimization techniques for segmentation in the level set framework and shape quantification techniques are discussed in Section VI. Finally, merits, demerits, the future and conclusions on level sets are discussed in Section VII.

II. Curve Evolution: Its Derivation, Analogies, and the Solution

Since this paper is focused on level sets, this section first presents the derivation of the fundamental equation of level sets, known as "curve evolution." Let $\Gamma(t)$ be the closed interface or front propagating along its normal direction (see Fig. 1, bottom). This closed interface $\Gamma(t)$: $[0, \infty) \rightarrow \Re^N$, can either be a curve in 2-D space or a surface in 3-D space. The main idea is to represent the front $\Gamma(t)$ as the *zero level set* of a higher dimensional function ϕ.

Let $\phi(x, t = 0)$, where $x \in \Re^N$ be defined by $\phi(x, t = 0) = d$, where d is the signed distance from position x to $\Gamma(0)$ and the

plus (minus) sign is chosen if the point x is outside (inside) the initial front $\Gamma(0)$. Thus an initial function is: $\phi(x, t = 0) = \Re^N \rightarrow \Re$ with the property: $\Gamma(t = 0) = (x|\phi(x, t = 0) = 0)$. The goal now is to produce an equation for the evolving function $\phi(x, t)$ so that ϕ always remains zero on the propagating interface. Let $x(t)$, $t \in [0, \infty)$ be the path of a point on the propagation front (see Fig. 1, bottom), i.e., $x(t = 0)$ is a point on the initial front $\Gamma(t = 0)$ and $x_t = V(x(t))$ with the vector x_t normal to the front at $x(t)$. Since the evolving function ϕ is always zero on the propagating front, thus $\phi(x(t), t) = 0$. By the chain rule

$$\phi_t + \sum_{i=1}^{N} \phi_{x_i} x_{i_t} = 0 \tag{1}$$

where x_i is the ith component of x. Since

$$\begin{aligned} &\sum_{i=1}^{N} \phi_{x_i} x_{i_t} \\ &\quad = (\phi_{x_1}, \phi_{x_2}, \phi_{x_3} \cdots \phi_{x_N}) . (x_{1_t}, x_{2_t}, x_{3_t} \cdots x_{N_t}) \\ &\quad = V(x(t))|\nabla\phi| \end{aligned} \tag{2}$$

hence, using (1) and (2), the final curve evolution equation is given as

$$\frac{\partial\phi}{\partial t} = V(\kappa)|\nabla\phi| \tag{3}$$

where ϕ is the level set function and $V(\kappa)$ is the speed with which the front (or *zero level curve*) propagates. This fundamental[5] equation describes the time evolution of the level set function (ϕ) in such a way that the *zero level curve* of this evolving function is always identified with the propagating interface. The term "level set function" will be interchangably be used with the term "flow field" or simply "field" during the course of this paper. The above equation is also called a Eulerian representation of evolution due to the work of Osher and Sethian [67]. Equation (3) for 2-D and 3-D cases can be generalized as: $\partial\phi/\partial t = V_\kappa(x, y)|\nabla\phi|$ and $\partial\phi/\partial t = V_\kappa(x, y, z)|\nabla\phi|$, respectively, where $V_\kappa(x, y)$ and $V_\kappa(x, y, z)$ are curvature dependent speed functions in 2-D and 3-D, respectively.

Three Analogies of the Curve Evolution Equation: 1) Note that these equations can be compared with the Euclidean geometric heat equation (see Grayson *et al.* [70]), given as: $\partial\mathcal{C}/\partial t = \kappa\mathcal{N}$, where κ is the curvature and $\mathcal{N}$ is the inward unit normal and $\mathcal{C}$ is the curve coordinates. 2) Equation (3) is also called the curvature motion equation, since the rate of change of the length of the curve is a function of $\partial\mathcal{C}/\partial t$. 3) The above equations can be written in terms of differential geometry using divergence as: $\partial\phi/\partial t = \nabla.(\nabla\phi/|\nabla\phi|)|\nabla\phi|$, where geometrical properties such as normal curvature ($\mathcal{N}$) and mean curvature ($\mathcal{H}$) are given as: $\mathcal{N} = \nabla\phi/|\nabla\phi|$ and $\mathcal{H} = \nabla.(\nabla\phi/|\nabla\phi|)$.

[5]Recently, Faugeras and his coworkers from INRIA (see Gomes *et al.*, [52]) modified (3) into the "preserving distance function" as

$$\frac{\partial\phi}{\partial t} = V(\mathbf{x})(\mathbf{x} - \phi\nabla\phi) \tag{4}$$

where $\mathbf{x}$ was the vector of x and y coordinates, ϕ is the signed distance function. The main characteristic of this equation was that ϕ and V are orthogonal to each other (see details by Gomes *et al.*, [52]).

A. The Eikonal Equation and Its Mathematical Solution

In this section, the mathematical solution is presented for solving the level set function with unity speed. Such a method is needed to compute the "signed distance transform" when the raw contour crosses the background grid. Consider a case of a "front" moving with a velocity $V = V(x, y)$, such that V is greater than zero. Using Osher–Sethian's [67] level set equation, consider a monotonically advancing front represented in the form: $\phi_t = V(x, y)||\nabla\phi||$, where ϕ_t is the rate of change of the level set and $\nabla\phi$ is the gradient of the ϕ. Let $T(x, y)$ be the time at which the front crosses the grid point (x, y). In this time, the surface $T(x, y)$ satisfies the equation: $||\nabla T||.V = 1$. By approximation[6] the solution to the Eikonal equation is

$$\begin{aligned} &[\mathbf{max}(\mathbf{max}(D^{-x}T, 0), -\mathbf{min}(D^{+x}T, 0))]^2 \\ &\quad + [\mathbf{max}(\mathbf{max}(D^{-y}T, 0), -\mathbf{min}(D^{+y}T, 0))]^2 \\ &\quad = \frac{1}{V^2{}_{xy}} \end{aligned} \tag{5}$$

where V^2_{xy} is the square of the speed at location (x, y) and $D^{-x}T$, $D^{+x}T$, $D^{-y}T$, $D^{+y}T$ are the backward and forward differences in time, given as

$$\begin{cases} D^{+x}T = \dfrac{T(x, y+1) - T(x, y)}{2} \\ \quad \&D^{-x}T = \dfrac{T(x, y) - T(x, y-1)}{2}, \\ D^{+y}T = \dfrac{T(x+1, y) - T(x, y)}{2} \\ \quad \&D^{-y}T = \dfrac{T(x, y) - T(x-1, y)}{2}. \end{cases} \tag{6}$$

There are efficient schemes for solving the Eikonal equation (3). For details, see Sethian *et al.* [71], Cao *et al.* [72] and Chen *et al.* [73]. Having discussed the taxonomy of level sets in medical imaging and the fundamental curve/surface evolution equation, the paper now presents the different types of level sets and their mathematical formalism along with their merits and demerits. Level sets without regularizers are discussed in Section III, and level sets fused with regularizers in the level set framework are discussed in Section IV.

III. Level Sets without Regularizers for Segmentation

The main characteristic of the level set is its ability to pick up the desired topology of the shape being segmented. The accuracy of the segmentation process depends upon when and where the propagating hypersurface needs to stop. Consider the special case of a surface moving with a speed $V > 0$. Let T be the time at which the surface crosses a given point. The function T then satisfies $|\nabla T|V = 1$. This equation simply says that the gradient of the arrival time is inversely proportional to the speed of the surface. If the propagating surface needs to stop close to the vicinity of the segmenting topological shape, then the speed of the surface should approximate closely to zero near the final segmenting shape. This means that gradient values at

[6]Numerical methodologies will be discussed in Section V.

the final shape boundary (in 2-D) or surface (in 3-D) should be very high (since the speed needed at the boundary is zero). Thus the accuracy of the segmentation process highly depends on how powerful the gradient values are at the final segmented shapes. This means the higher the gradient value, the faster the propagation of the curve/surface is, which results in a strong clamping force. As a result, one has robust and accurate segmentation. Thus the "stopping force" seen for the propagating surface is strongly dependent upon the gradient change of the final shape to be segmented. In the next few sections, several kinds of stopping forces[7] will be discussed in the class of "level sets without regularizers" or "implicit deformable models."

The layout of this section is as follows: Section III-A presents the stopping force due to the image gradient. Section III-B presents the stopping force due to edge strength. Section III-C presents the stopping force due to area minimization. Section III-D presents the stopping force due to mean curvature flow (MCF). Finally, in curvature dependent level sets, we discuss the work on 1) plain curvature and 2) mean curvature flow integrated with directionality.

A. Level Sets With Stopping Force Due to the Image Gradient (Caselles)

Using Osher and Sethian's [67] approach, Caselles *et al.* [75], Chopp *et al.* [42] and Rouy *et al.* [76] proposed the geometric active contours[8] followed by Malladi *et al.* [77]. The model proposed by Caselles and Malladi was based on the following equation: if $\phi(\mathbf{x}, t)$ was a 2-D scalar function that embedded the *zero level curve*, then the geometric active contour was given by solving

$$\frac{\partial \phi}{\partial t} = \underbrace{c(\mathbf{x})}_{\text{stopping-term-type-1}} (\kappa + V_0)|\nabla \phi| \tag{7}$$

where

- κ was the level set curvature;
- V_0 was the constant;
- $c(\mathbf{x})$ was the stopping term (type-1) based on the image gradient;

and was given as

$$c(\mathbf{x}) = \frac{1}{1 + |\nabla[G_\sigma(\mathbf{x}) * I(\mathbf{x})]|}. \tag{8}$$

Note that (7) is the same as (5) from Malladi *et al.* [78]. Rewriting (5) from Malladi *et al.* [78], the stopping force becomes

$$c(\mathbf{x}) = e^{\alpha |\nabla[G_\sigma(\mathbf{x}) * I(\mathbf{x})]|} \tag{9}$$

where α was the gradient constant and $|\nabla[G_\sigma(\mathbf{x}) * I(\mathbf{x})]|$ was the absolute of the gradient of the convoluted image. This convolved image was computed by convolving the original image by the Gaussian function with a known standard deviation σ. Taking the constant α as unity and using the exponential series, one can obtain equation (8) from equation (9).

[7]Also called the data consistency term in the level set framework.

[8]Or the level set or curve evolution equation.

Pros and Cons of Caselles' Work: Although Caselles and Malladi's work was able to solve this problem, it had the following weaknesses: 1) The stopping term was not robust and hence could not stop the bleeding or leaking of the boundaries. 2) The pulling back feature was not strong. This meant that if the front propagated and crossed the goal boundary, then it could not come back.

B. Level Sets With Stopping Force Due to Edge Strength $(\nabla c.\nabla \phi)$ (Yezzi)

Kichenassamy *et al.* [74] and Yezzi *et al.* [51] tried to solve the above problems by introducing an extra stopping term (type-2), also called the pull back term. This was expressed mathematically as

$$\frac{\partial \phi}{\partial t} = c(\mathbf{x})(\kappa + V_0)|\nabla \phi| + \underbrace{(\nabla c.\nabla \phi)}_{\text{stopping-term-type-2}}. \tag{10}$$

Note that $(\nabla c.\nabla \phi)$ denoted the projection of an attractive force vector on the normal to the surface. This force was realized as the gradient of a potential field c. This potential field c for the 2-D and 3-D case was given as: $c(x, y) = -|\nabla G_\sigma * I(x, y)|$ and $c(x, y, z) = -|\nabla G_\sigma * I(x, y, z)|$, respectively. Note that equation (10) is similar to equation (7) given by Malladi in [78]. Malladi *et al.*calls the equation as an additional constraint on the surface motion ϕ_t. Rewriting [78, eq. (7)] we have

$$\phi_t + c(\mathbf{x})(\epsilon\kappa + V_0)|\nabla \phi| - \beta(\nabla c.\nabla \phi) = 0 \tag{11}$$

where

- β was the edge strength constant;
- V_0 was a constant (1 as used by Malladi *et al.*);
- κ was the curvature dependent speed;
- ϵ was the constant term controlling the curvature dependent speed;
- $(\nabla c.\nabla \phi)$ was the same as defined above.

Pros and Cons of Kichenassamy et al. [74] and Yezzi et al.'s [51] Methods: The weakness of the above technique was: 1) It still suffered from boundary leaking for complex structures, as pointed out by Siddiqui *et al.* [79].

C. Level Sets With Stopping Force Due to Area Minimization (Siddiqui)

Siddiqui *et al.* [79], [80] then changed Kichenassamy *et al.* [74] and Yezzi *et al.*'s [51] model by adding an extra term to it

$$\frac{\partial \phi}{\partial t} = c(\mathbf{x})(\kappa + V_0)|\nabla \phi| + (\nabla c.\nabla \phi) + \underbrace{\frac{V_0}{2}\mathbf{x}.\nabla c|\nabla \phi|}_{\text{stopping-term-type-3}} \tag{12}$$

where $(V_0/2)\mathbf{x}(\nabla c)|\nabla \phi|$ was the area minimizing term and was mathematically equal to the product of the divergence of the stopping term times the gradient of the flow. This term provided an additional attraction force when the front was in the vicinity of an edge.

Pros and Cons of the Area Minimization Technique: The major advantage of this technique was: 1) It performed better compared to the first and second implicit models. The major

weaknesses were: 1) The system was not very robust at handling the convolutedness of medical shapes. 2) The system did not take advantage of the regional neighborhood for the propagation or evolution of level sets. To some extent, this weakness was temporarily removed using multiple level sets (see Niessen *et al.* [60]), however this was not a robust solution to the segmentation of complex shapes such as in brain cortical segmentation.

D. Level Sets With Curvature Dependent Stopping Forces

The layout of this section is as follows: Plain curvature-driven techniques are presented in Section III-D-1. Integrating the directionality into mean curvature flow is presented in Section III-D-2. Note that the work on 3-D bubbles and free form deformations will not be discussed in this paper.

1) 3-D Geometric Surface-Based Cortical Segmentation (Malladi): The dominance of 3-D shape modeling using Geodesics active surfaces started with the UCLA group (see Osher and Sethian [67], Chopp *et al.* [3]) and then later used by the Berkeley Lab (see Malladi and Sethian, [78], [49]). Malladi's method was simply an extension from 2-D to 3-D of equations (7) and (8) and an additional term, the so-called gradient of the potential field. Thus, if: $\partial\phi/\partial t = c(\mathbf{x})(\kappa+V_0)|\nabla\phi|$, where κ is the level set curvature, V_0 is the constant and $c(\mathbf{x})$ was the stopping term based on image gradient and given as: $c(\mathbf{x}) = 1/(1 + |\nabla[G_\sigma(\mathbf{x}) * I(\mathbf{x})]|)$. Then Malladi's final equation for cortical segmentation was:

$$\frac{\partial\phi}{\partial t} = \underbrace{c(\mathbf{x})(\epsilon\kappa + V_0)|\nabla\phi|}_{\text{gradient+curvature+stopper}} + \underbrace{\beta\,\nabla\mathbf{P}.\nabla\phi}_{\text{attractive-force}} \tag{13}$$

where $\mathbf{P}$ was the gradient of the potential field given as: $\mathbf{P}(x, y, z) = |(\nabla(G_\sigma * I(x, y, z)))|$. Note that the term $\nabla\mathbf{P}.\nabla\phi$ denoted the projection of an attractive force on the surface normal. β controlled the strength of the attractive force. Also note that $V_0 = 1$ and κ was premultiplied by ϵ which controlled the mean curvature. The mean curvature κ in 3-D was: $\kappa = 1/((\phi_x^2+\phi_y^2+\phi_z^2)^{3/2})((\phi_{yy}+\phi_{zz})\phi_x^2+(\phi_{xx}+\phi_{zz})\phi_y^2+(\phi_{xx}+\phi_{yy})\phi_z^2 - 2(\phi_x\phi_y\phi_{xy} + \phi_x\phi_z\phi_{xz} + \phi_y\phi_z\phi_{yz}))$. So, the deformation was focused more on propagation based on curvature rather than on stopping force.

Pros and Cons of Malladi's Technique: The major advantages of this technique were: 1) This technique was one of the first in the application of level sets in the medical imaging world. 2) The recent work of Malladi *et al.* [78], [49] applied level sets for brain segmentation and showed the speed was $N\log(N)$, where N was the total number of points in the data set. The major disadvantages of this technique were: 1) It was not clear from this paper how the value of the arrival time T was selected to segment the cortex accurately, but their protocol followed a two-step process. They first reconstructed the arrival time function using the fast marching method (see Sethian *et al.* [71], [114]). Then, they treated the final $T(x, y, z)$ function as an initial condition to their full model. This meant that they solved $\partial\phi/\partial t = c(\mathbf{x})(\epsilon\kappa+V_0)|\nabla\phi|$ in a few time steps using the finite difference with $\phi(x, y, z; t = 0) = T(x, y, z)$. 2) The system was not robust and did not take advantage of the region-based analysis. The modification of this technique will be seen in Section IV, where four systems are presented with the design of propagation forces, a key to the success of robust segmentation.

2) Curvature Dependent Force Integrated with Directionality (Lorigo): Recently, Lorigo *et al.* [81] presented an algorithm for brain vessel reconstruction based on curve evolution in 3-D, also know as "codimension two" in geodesic active contours. This method used two components: 1) mean curvature flow (MCF) and 2) the directionality of vessels. The mean curvature flow component was used to derive the Eulerian representation of the level set equation. If ϕ was the SDT and $\lambda(\nabla\phi(\mathbf{x}, t), \nabla^2\phi(\mathbf{x}, t))$ are the eigen values of the projection operator: $\mathcal{P}_{\nabla\phi}\nabla^2\phi P_{\nabla\phi}$, where $\mathcal{P} = I - (qq^T/|q|^2)$ and q was a nonzero vector, then using these eigenvalues, the Eulerian representation of the curve evolution was given by Lorigo as: $\partial\phi/\partial t = \lambda(\nabla\phi(\mathbf{x}, t), \nabla^2\phi(\mathbf{x}, t))$. The second component was the normal of these vessels projected onto the plane and was given as the product of $\nabla\phi$ with the projection vector d. This projection vector was computed using the Hessian of the intensity image, I and was given as: $(g'/g)(H(\nabla I/|\nabla I|))$, where g was the edge detector operator. Adding these two components, the complete level set equation was

$$\frac{\partial\phi}{\partial t} = \underbrace{\lambda(\nabla\phi(\mathbf{x}, t), \nabla^2\phi(\mathbf{x}, t))}_{\text{mean-curvature-force}} + \underbrace{D \times S \times \frac{g'}{g}\left(H\frac{\nabla I}{|\nabla I|}\right)}_{\text{Angular-Balloon-force}} \tag{14}$$

where D was the directionality term which was the dot product of $\nabla\phi$ and ∇I which was the angle between these two vectors. S was the scale term. Note that the second term was like an angular balloon force which navigated the deformation process.

Pros and Cons of Lorigo's Technique: The major advantages of this technique were: 1) The method successfully demonstrated the segmentation of these vessels of the brain. 2) The method used the directional component in the level set framework, which was necessary for segmenting twisted, convoluted and occluded vessels. 3) The technique was used to compute vessel radii, a clinically useful measurement. The weaknesses of Lorigo's work were: 1) Not much discussion was available on the computation of the scale factor S. 2) The method has yet to show the analytical model since the output of the system showed relatively thinner vessels compared to maximum intensity projection (MIP)[9] and thresholding schemes. 3) There was no comparison made between segmented results and the ground truth hence, this was not validated. So, we saw that the class of "level set without regulizers" primarily focused on stopping the deformation process by using the data consistency term, $c(\mathbf{x})$, or propagating the deformation process totally based on curvature-dependent speed. None of the above methods took advantage of the region-based strategy of neighborhoods, hence they were not successful in capturing complex shapes of medical objects/organs such as brain cortex. The next section is focused on demonstrating the design of the propagating force based on region-strategy which is fused into the level set fundamental model to improve the robustness of the segmentation for medical imagery.

[9]The MIP algorithm is a very popular technique. An example can be seen by Suri *et al.* [83].

IV. Level Sets Fused With Regularizers for Segmentation

Fusing regional statistics into parametric or geometric boundary/surfaces has brought a major success in medical imaging (see the recent work by Yezzi *et al.* [88], Guo *et al.* [89], Leventon *et al.* [117], Lorigo *et al.* [82] and recently by Suri *et al.* [55], [56]). The main reason for this was that the segmentation system took advantage of the local and global shape information for pulling and pushing boundaries/surfaces to capture the topology in the level set framework based on PDE. Incorporating such regional-statistics, also known as "level sets with regularizers," makes the overall segmentation system more robust and accurate.

This section presents four different medical segmentation systems where regularizers are fused with geometric contour or geodesic active contours in the level set framework. Section IV-A presents the derivation of geodesic active contours from parametric deformable models. The same section shows the design of the propagation force using fuzzy clustering, which was later fused in geodesic active contours or level sets. Section IV-B presents 3-D constrained level sets where two propagating surfaces are coupled by a constraint. The methodology of computing the propagation force using Bayesian statistics is shown in Section IV-C. Section IV-D presents the fusion of the shape-based information as a propagating force in the level set formalism. Finally, a comparison among the designs of different propagation forces and their uses in level sets will be discussed in Section IV-E.

A. 2-D Regional Geometric Contour: Design of Regional Propagation Force Based on Clustering and Its Fusion With Geometric Contour (Suri/Marconi)

Recently, Suri [2], [55], [56] derived the curve evolution equation by embedding the region statistics into the parametric classical energy model. This method was in the spirit of Xu *et al.*'s [90] attempt. Part of that derivation[10] will be discussed here (for details see Suri *et al.* [1]). To start with, the standard dynamic classical energy model as given by Kass *et al.* [66] was

$$\gamma \frac{\partial \mathbf{X}}{\partial t} = \underbrace{\frac{\partial}{\partial s}\left(\alpha \frac{\partial \mathbf{X}}{\partial s}\right) - \frac{\partial^2}{\partial s^2}\left(\beta \frac{\partial^2 \mathbf{X}}{\partial s^2}\right)}_{\text{internal-energy}} + \underbrace{F_{ext}(\mathbf{X})}_{\text{external-energy}} \tag{15}$$

[10]Aubert *et al.* [91] recently tried to give some remarks between classical snakes (given first by Kass *et al.* [66]) and geodesic snakes (given first by Caselles *et al.* [87]). Aubert *et al.* showed that the above two models are only valid for curves with a fixed length using the definition that "classical snakes and geodesic snakes are equivalent, if they have same extremas." Aubert *et al.* also showed that Mauperthuis' principle is not enough to show the equivalence between classical snakes and geodesic snakes. Aubert *et al.* mathematically showed that the derivation of the gradient flow from the classical snake and the geodesic snake have different expressions if Caselles *et al.*'s definition was used for developing the equivalence. Aubert *et al.* did, however, show equivalence between these two energy models to be the same if the following definition was used for equivalence: "Two minimization problems are equivalent if the direction which locally most decreases a criterion is also a decreasing direction for the other criterion and vice versa." In the forthcoming derivation, Caselles' idea was used for establishing equivalence between parametric and geodesic models.

where $\mathbf{X}$ was the parametric contour and γ was the damping coefficient. As seen in (15), the classical energy model constituted an energy-minimizing spline guided by external and image forces that pulled the spline toward features such as lines and edges in the image. The energy-minimizing spline was named "snakes" because the spline softly and quietly moved while minimizing the energy term. The internal energy was composed of two terms: the first term was the first-order derivative of the parametric curve which acted like a membrane and the second term was the second derivative of the parametric curve which acted as a thin plate (also called the pressure force). These terms were controlled by elastic constants α and β. The second part of the classical energy model constituted the external force given by $F_{ext}(\mathbf{X})$. This external energy term depended upon image forces which were a function of image gradient. Parametric snakes had flexibility to dynamically control movements, but there were inherent drawbacks when they were applied to highly convoluted structures, sharp bends and corners, or on images with a large amount of noise. Suri *et al.* [1], [2], [64] and [57] tried to preserve the classical properties of these parametric contours but also brought these geometric properties which could capture the topology of convoluted shapes (say, cortical WM and GM). Since the curve evolution when embedded with regional statistics was the fundamental equation in the design of a propagation force, thus, the derivation will be presented next.

Derivation of the Geometric Snake: Since the second derivative term in (15) did not significantly affect the performance[11] of active geometric snakes (see Caselles *et al.* [87]), Suri dropped that term and replaced it with a new pressure force which was given by: $F_p(\mathbf{X})$. This pressure force was an outward force which was a function of the unit normal, $\mathcal{N}$ of the deforming curve. Suri defined the pressure force as: $F_p(\mathbf{X}) = w_p(\mathbf{X})\mathcal{N}(\mathbf{X})$, thus the new parametric active contour could be rewritten by replacing $\beta(\partial^2\mathbf{X}/\partial s^2)$ by $w_p(\mathbf{X})\mathcal{N}(\mathbf{X})$, resulting in

$$\gamma \frac{\partial \mathbf{X}}{\partial t} = \underbrace{\frac{\partial}{\partial s}\left(\alpha \frac{\partial \mathbf{X}}{\partial s}\right)}_{\text{smoothing-force}} - \underbrace{w_p(\mathbf{X})\mathcal{N}(\mathbf{X})}_{\text{pressure-force}} + \underbrace{F_{ext}(\mathbf{X})}_{\text{external-force}} . \tag{16}$$

By redefining $(\partial/\partial s)(\partial\mathbf{X}/\partial s)$ to be the curvature κ, and readjusting the terms by defining the constants $\epsilon = \alpha/\gamma$, $V_p = (w_p(X)/\gamma)\mathcal{N}(\mathbf{X})$ and $V_{ext} = F_{ext}/\gamma$, thus (16) was rewritten as: $\partial\mathbf{X}/\partial t = (\epsilon\kappa + V_p + V_{ext}.\mathcal{N})\mathcal{N}$. The above was analogous to Osher and Sethian's [67] equation of curve evolution, given as: $\partial\phi/\partial t = V(\kappa)\mathcal{N}$, where $\mathcal{N} = -(\nabla\phi/|\nabla\phi|)$. Note, ϕ was the level set function and $V(\kappa)$ was the curvature dependent speed with which the front (or *zero level curve*) propagated. The expression $\partial\phi/\partial t = V(\kappa)\mathcal{N}$ described the time evolution of the level set function (ϕ) in such a way that the *zero level curve* of this evolving function was always identified with the propagating interface. Comparing $\partial\mathbf{X}/\partial t$ and $\partial\phi/\partial t = V(\kappa)\mathcal{N}$, and using the geometric property of the curve's normal $\mathcal{N}$ and considering only the normal components of internal and external forces, $(\partial/\partial s)(\alpha(\partial\mathbf{X}/\partial s))\mathcal{N} = (\alpha\kappa)$, Suri obtained the level

[11]See the previous footnote.

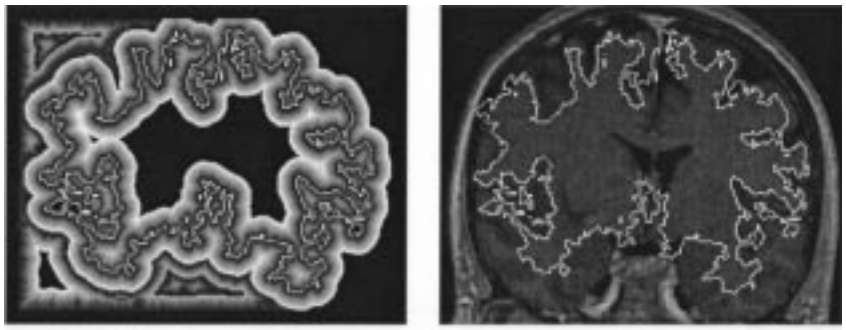

(a) (b)

Fig. 2. (a) Results of the superimposition of the ZLC and its level set function using the "fast marching method" in the narrow band (NB). Tube reconstruction. (b) Segmented GM boundary (results, courtesy of Jasjit Suri, Marconi Medical Systems, Inc. For details, see [55] and [56]).

set function (ϕ) in the form of a partial differential equation (PDE) as

$$\frac{\partial \phi}{\partial t} = (\epsilon\kappa + V_p)\,|\nabla\phi| - V_{ext}.\nabla\phi. \tag{17}$$

Note, V_p was considered as a regional force term and was mathematically expressed as a combination of the inside-outside regional area of the propagating curve. This was defined as $w_R/\gamma R$, where R was the region indicator term that fell between zero and one (the design of this propagation force will be seen in the next section). So, the above derivation showed that the regional information was one of the factors which controlled the speed of the geometric snake or propagating curve in the level set framework. A framework in which a snake propagated by capturing the topology of the WM/GM, navigated by the regional, curvature, edge and gradient forces, was called regional geometric snakes. Also note that (17) had three terms: the product of ϵ and κ, V_p, and V_{ext}. These three terms were the speed functions which controlled the propagation of the curve. These three speed functions were known as curvature, regional, and gradient speed functions, since they contributed toward the three kinds of forces responsible for curve deformation.

1) Design of the Propagation Force Based on Fuzzy Clustering: Having discussed the embedding of the regional-force function in the level set framework in the previous section, this section now presents how this regional force V_p was computed that navigated the deformation process for the final segmentation of the convoluted topology. As defined previously, the regional propagation force was mathematically given as: $w_R/\gamma R$, where R was the region indicator term that fell between zero and one. An example of such a region indicator was from a membership function of the fuzzy classifier. Thus Suri expressed the region indicator term as: $R_{ind} = 1 - 2u(x, y)$, where $u(x, y)$ was the fuzzy membership function which had a value between zero to one. R_{ind} was the region indicator function and fell in the range between -1 to $+1$. This membership function $u(x, y)$ was computed based on the fuzzy principle (see Bezdek *et al.* [93]).

Fig. 3 (left) shows the system used for GM boundary estimation, whose results can be seen in Fig. 2. Note that the last stage was the isocontour extraction. This was accomplished using an isocontour algorithm at subpixel resolution (for details on these methods, see Berger *et al.* [95], Sethian *et al.* [96], Tababai *et al.* [97], Huertas *et al.* [98] and Gao *et al.* [99]).

Pros and Cons When Clustering Was Used as a Regularizer: The major advantages of embedding the clustering technique as a regularizer in the level set framework were: 1) robust implementation; 2) accurate boundary estimation depending upon the class chosen; 3) ease of implementation. The major weaknesses of this method were: 1) The algorithm was not fast enough to be implemented for real-time applications. 2) The performance of the algorithm depended upon a few parameters, such as: the error threshold and the number of iterations. 3) The choice of the initial cluster was important and needed to be carefully selected. 4) The algorithm was not very robust to MR images which had spatial variations due to large RF inhomogeneities.

B. 3-D Constrained Level Sets: Fusion of Coupled Level Sets With Bayesian Classification as a Regularizer (Zeng/Yale)

Coupled constrained boundary estimation in medical imaging has been very successful when applying to shape analysis (see the derivation in the appendix by Suri *et al.* [64], where end diastole (ED) and end systole (ES) shapes of the left ventricle (LV) were subjected to the "coupled constrained principle." These constraints were computed based on eigenvalues). In the level set framework, Zeng *et al.* [100], [54] recently had put the level set under constraints in neurological applications. For example, a volume has three tissue types, say T1, T2, and T3, and say tissue T2 was embedded in between tissues T1 and T3. Such an example is seen in the human brain where the GM is embedded between the WM and CSF. There is a coupling between WM–GM and GM–CSF volumes. Zeng's method had used constrained level sets in the application of human cortex segmentation from MR images. The proposed coupled level set formulation was motivated by the nearly constant thickness of the cortical mantle and took this tight coupling as an important constraint. The algorithm started with two embedded surfaces in the form of concentric sphere sets. The inner and outer surfaces were then evolved, driven by their own image-derived information, respectively, while maintaining the coupling in between through a thickness constraint.

1) Overall Pipeline of Coupled Constrained Level Set Segmentation System: The cortical segmentation system based on level sets which was constrained by the coupling between the

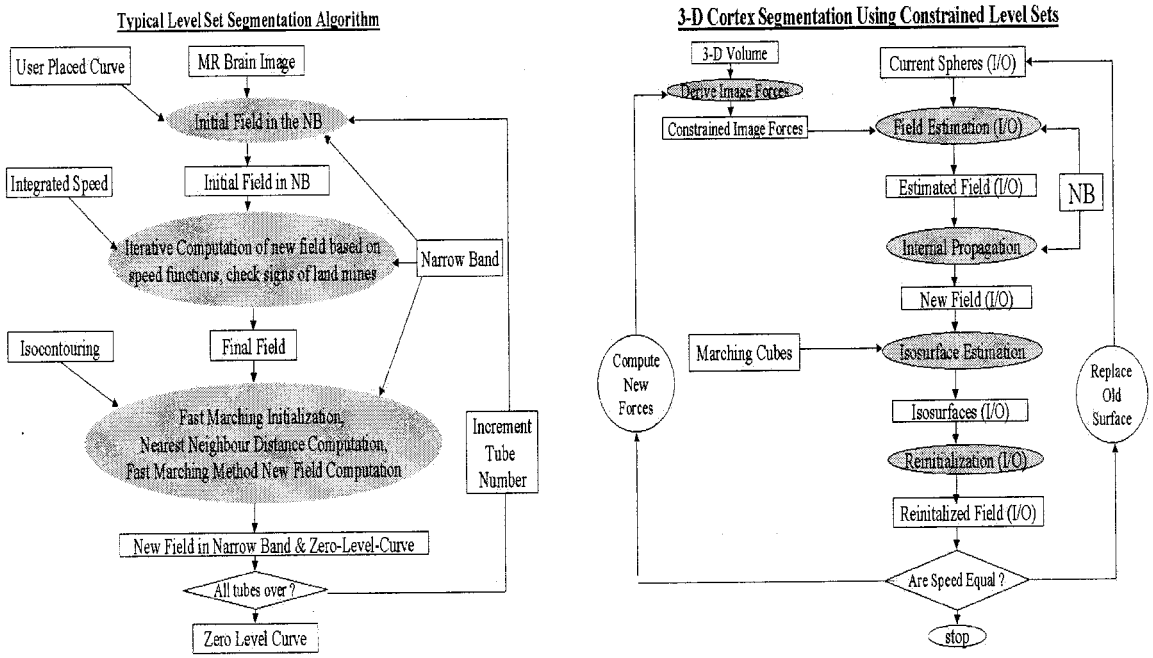

(a) (b)

Fig. 3. (a) Typical level set segmentation algorithm. This can be applied for brain segmentation. In such a case, the integrated speed will have regional, gradient and curvature speed terms. Note: the paradigm uses the fast marching method in the narrow band. (b) Constrained level set application: cortex segmentation algorithm. The user first specifies the initial spheres. Using the distance transform based on the shortest distance, the initial field is estimated in the narrow band. The surface is propagated in the narrow band and the new field distribution is estimated taking the propagation forces into account. These forces are computed using the likelihood measure. Using the marching cube algorithm, the *zero level surface* is computed, also known as isosurface extraction. The surfaces are reinitialized and the speeds of two new isosurfaces are compared. If they are equal to zero, the system stops the propagation, or else the next round is iterated. Before the new field is estimated in the next round, the constrained forces are derived again.

WM–GM and GM–CSF volumes can be seen in Fig. 3 (right). This system will be briefly discussed next, since it has clinical value in neurological analysis. The input of the system was the 3-D gray scale volume and the initial spheres. From the gray scale volume, the propagating forces[12] were computed. This was called the likelihood function which drove the field distributions (to be discussed in Section IV-B2). From the initial concentric spheres, the initial field was computed in the narrow band. Zeng *et al.* [54] then computed the new field driven by these propagating forces in this narrow band. This was where Zeng *et al.* ran the *coupled level set* equations (to be discussed in Section IV-B3). From this new field the new surface was computed, known as the isosurface, which represented a unisurface value based on Marching Cubes (see Lorensen *et al.* [102]). The algorithm performed the reinitialization and was ready to repeat the above steps if the external and internal speeds of the spheres were not equal to zero. The algorithm used the fast marching method in the narrow band to optimize the performance. Thus a final representation of the cortical bounding surfaces and an automatic segmentation of the cortical volume was achieved. The intermediate and final results of the above coupled constrained level set algorithm can be seen in Fig. 4. The following three sections will discuss each of these components of this pipeline.

2) Design of the Propagation Force Based on the Bayesian Model: Capturing gray scale edges of the WM/GM interface and GM/CSF interface was a very critical component in the entire system. The image-derived information was obtained by using a local likelihood operator based on gray-level information rather than on image gradient alone, which gave the algorithm the ability in capturing the homogeneity of the tissue inside the volumetric layer. First, the 3-D field distribution[13] was estimated given the initial spheres.[14] From the initial field distribution, the normals and offsets at every voxel location were computed using the level set framework. These two offsets to a central voxel gave information on the neighboring voxels. The first set of voxels belonged to the first distribution, while the second set of voxel belonged to the second distribution. Next, the likelihood values were computed using these two distributions. For the first distribution (here, WM), the WM likelihood probability was computed given a voxel and similarly, the GM likelihood was computed given the second distribution (here, GM). Assuming the distributions to be independent, the GM–WM likelihood computation was mathematically given as

$$p_{\text{GM–WM}} = \prod_{g \in G} \frac{1}{\sqrt{2\pi\sigma_G}} \exp\left(-\frac{(I_g - \mu_G)^2}{\sigma_G^2}\right) \cdot \prod_{w \in W} \frac{1}{\sqrt{2\pi\sigma_W}} \exp\left(-\frac{(I_w - \mu_W)^2}{\sigma_W^2}\right) \quad (18)$$

where

W and G were the WM and GM regions;
μ_W and μ_G were mean values of the WM and GM regions;

[12]Also known as steering engines or image forces.

[13]Signed distance transform.

[14]Inside and outside spheres.

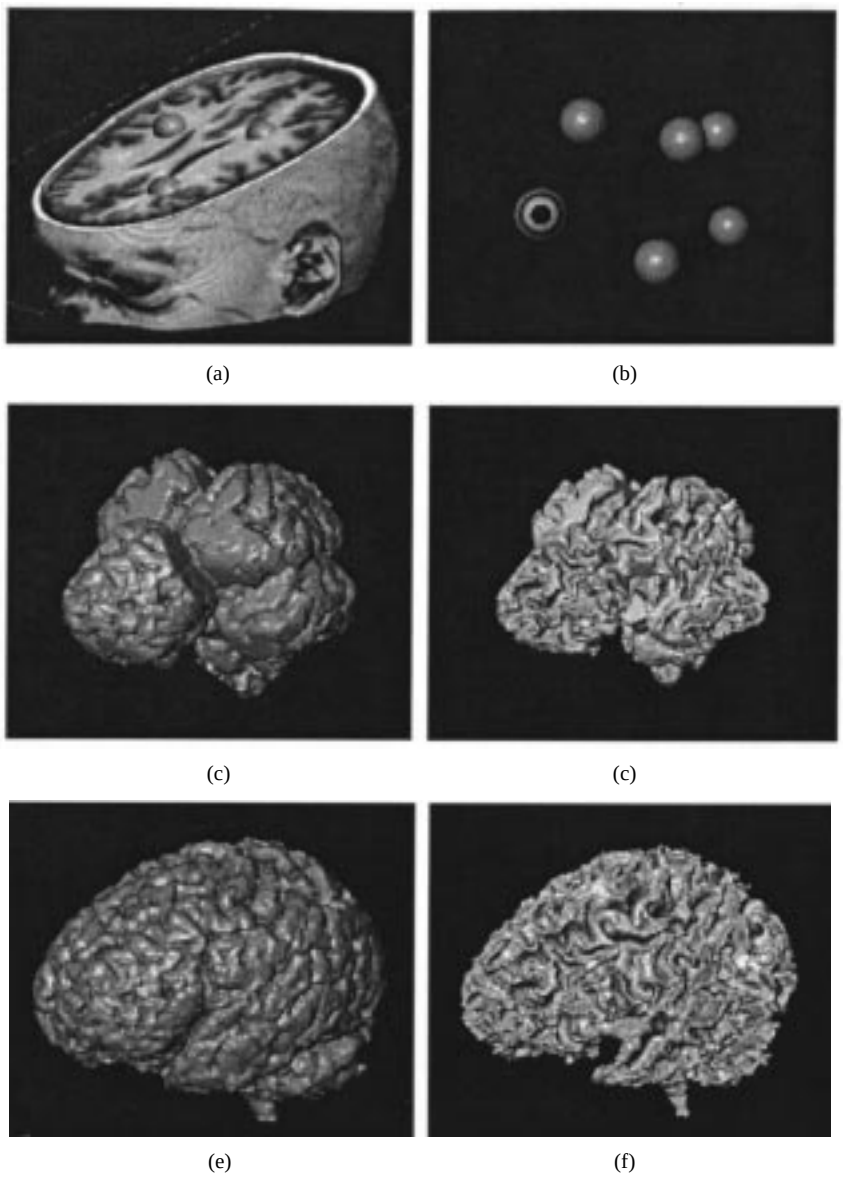

Fig. 4. Propagation of the outer and inner bounding surfaces. (a) Embedded sphere sets as initializations shown in unedited 3-D MR brain volume. (b) Outer and inner bounding spheres. (c) Intermediate step in GM surface propagation. (d) Intermediate step in WM surface propagation. (e) Final result of the segmented GM/CSF surface. (f) Final result of the segmented WM/GM surface (Courtesy of Xiaolan Zeng, R2 Technology, Inc.).

σ_W^2 and σ_G^2 were standard deviations of the WM and GM regions;

I_w and I_g were the WM and GM pixel intensities.

Note, the output of the GM–WM likelihood function was the image which had edge information about the boundary of the GM–WM. Similarly, the WM–CSF likelihood function was an image which had the WM–CSF edge or gradient information.

3) Constrained Coupled Level Sets Fused With Bayesian Propagation Forces: The propagation of surfaces toward the final goal surface was performed in the level set framework. Instead of evolving two surface directly, two level functions whose *zero level set* corresponding to the cortical bounding surfaces were calculated. The equations of these evolving surfaces were

$$\begin{cases} \psi_{\text{in}}(t) + F_{\text{in}}|\nabla\psi_{\text{in}}| = 0 \\ \psi_{\text{out}}(t) + F_{\text{out}}|\nabla\psi_{\text{out}}| = 0. \end{cases} \tag{19}$$

The coupling between these two surfaces was realized through propagation speed terms F_{out} and F_{in} which are dependent on the distance between the two surfaces and the propagation forces computed above. While the distance between the two surfaces was within the normal range, the inner and outer cortical surfaces propagated according to their own image features. When the distance started to fall out of the normal range, the propagation slowed down and finally stopped only when the distance was outside the normal range, or the image feature was strong enough. A coupled narrow band algorithm was customized for the coupled-surfaces propagation. The correspondence between points on the two bounding surfaces falls out automatically during the narrow band rebuilding, which was required for surface propagation at each iteration. This shortest distance-based correspondence was essential in imposing the coupling between two bounding surfaces through the thickness constraint. Once the new field was computed, the

isosurface was extracted based on the marching cube technique (see Lorensen *et al.* [102]). Having discussed all the stages of the constrained coupled segmentation system, next will be presented in pros and cons.

Pros and Cons of Coupled Level Sets Fused With Bayesian Classification: The coupled-surfaces propagation with the level set implementation offered the following advantages: 1) easy initialization; **2**) computational efficiency (one hour); 3) the ability to handle complex sulcal folds; 4) simultaneous "skull-stripping" (delineation of nonbrain tissues) and GM/WM segmentation; 5) ready evaluation of several characteristics of the cortex, such as surface curvature and a cortical thickness map; 6) integration of efficiency and flexibility of level set methods with the power of shape constraint; 7) a promise toward the improved accuracy of brain segmentation through extensive experiments on both simulated brain images and real data. The major weaknesses were: 1) The method did not include a model that dealt with image inhomogeneity, unlike other research such as that of Wells *et al.* [101]; 2) the technique imposed no constraint to preserve the cortical surface topology, however it did take advantage of the topological flexibility of level set methods; and 3) the resulting surface may not produce a 2-D manifold. Other research work using coupled level sets was done by Gomes *et al.* [52].

C. 3-D Regional Geometric Surface: Fusion of the Level Set With Bayesian-Based Pixel Classification Regularizer (Barillot/IRISA)

Baillot *et al.* [103], [104] and [105] recently designed the brain segmentation system based on the fusion of region into boundary/surface estimation. This algorithm was quite similar in approach to Suri's method discussed previously in Section IV-A. This algorithm was another instance where the propagation force V_0 in the fundamental level set segmentation equation $\phi/\partial t = c(\mathbf{x})(\kappa + V_0)|\nabla\phi|$ was changed into a regional force. There were in all three changes made to this equation by Barillot *et al.* First was in the propagation force V_0, second was in the data consistency term or stopping term $c(\mathbf{x})$, and the third change was on the step size Δt. These equations and their interpretation will be briefly discussed next.

1) Design of the Propagation Force Based on Probability Distribution: The key idea was to utilize the probability density function inside and outside the structure to be segmented. The pixel/voxel in the neighborhood of the segmenting structure was responsible for creating a pull/push force on the propagating front. This was expressed in the form of the probability density function to be estimated inside the structure, $p_i(u)$, the probability density function to be estimated outside the structure, $p_e(u)$ and the prior probability for a voxel to be inside the structure. Note here, u[15] was the intensity value of a voxel at location (x, y, z). Using the above concept, this bidirectional propagation force was estimated as:

$$V_0 = \text{sgn}\{\alpha_i\, p_i(u) - (1-\alpha_i)\, p_e(u)\} \tag{20}$$

[15]Note, this symbol is not to be confused with the membership function used in Section IV-A.

where sgn(x) was 1 if $x \geq 0$ and was -1 if $x < 0$. The second modification was to the data consistency term[16] that changed from the gradient term into the extended gradient term. This term was changed from $c(\mathbf{x}) = 1/(1+|\nabla[G_\sigma(\mathbf{x}) * I(\mathbf{x})]|)$ to a term which was based on the transitional probability of going from inside to outside the object to be segmented. This was mathematically given as: $c(\mathbf{x}) = g[p_T(x|I, C)]$, where $g[x]$ was $1-4x^3$ if $x < 0.5$ and was $4(1-x)^3$, if $x \geq 0.5$. The term p_T was computed based on these three parameters: α_i, $p_i(u)$ and $p_e(u)$, and mathematically estimated if the probability of a pixel/voxel class C belonged to a set inside and outside the object. If the class C was inside the region, then p_T was given as $((1-\alpha_i)p_e(I(x)))/(\alpha_i p_i(I(x)) + (1-\alpha_i)p_e(I(x)))$, while it was $((\alpha_i)p_i(I(x)))/(\alpha_i p_i(I(x)) + (1-\alpha_i)p_e(I(x)))$ if C was outside, derived from the simple Bayesian rule.

Pros and Cons of Baillard/Barillot's Technique: The major advantages of this technique were: 1) The paper was an excellent example of the fusion of region-based information into the boundary/surface. 2) The results were very impressive; however, it would have been valuable to see the enlarged version of the results. 3) The algorithm was adaptive since the data consistency term ($c(\mathbf{x})$) and the step size (Δt) were adaptively estimated in every iteration of the front propagation. This provided a good tradeoff between convergence speed and stability. 4) This method used stocastic-EM (SEM) instead of expectation-minimization (EM), which was a more robust and accurate method for estimation of probability density function parameters. 5) The method had been applied to various brain structures and to various imaging modalities such as ultrasound. 6) The algorithm hardly needed any tuning parameters and thus it was very efficient. Both methods (Suri's and Baillard's) were designed to control the propagation force using region-based analysis. Suri's method used regional-force computed using pixel-classification based on clustering, while Baillard *et al.*'s method used pixel-classification based on Bayesian-statistics.

D. 2-D/3-D Regional Geometric Surface: Fusion of Level Set With Global Shape Regularizer (Leventon/MIT)

Another application of the fusion of Bayesian statistics into geometric boundary/surface to model the shape in the level set framework was done recently by Leventon *et al.* [117]. Though this technique did not show the segmentation of the cortex, rather it focused on the segmentation of the subcortical area such as the corpus callosum, and was a good example of the fusion of the boundary and region-based technique. Leventon *et al.* derived the shape information using maximum *a posteriori* probability (MAP) and fused that with gradient and curvature driven boundary/surface in the level set framework. This MAP mode of shape used *priors* in the Bayesian framework from the training data set (analogous to Cootes *et al.*'s [118] technique). Using (10), the level set curve/surface evolution was given as

$$\frac{\partial\phi}{\partial t} = c(\mathbf{x})(\kappa + V_0)|\nabla\phi| + \underbrace{(\nabla c.\nabla\phi)}_{\text{extra-stopping-term}}. \tag{21}$$

[16]Or stopping term.

Note that this equation was exactly the same as (8) used by Leventon *et al.* in [117], whose solution using finite difference was:

$$\phi(t+1) = \phi(t) + \lambda_1 \left[\underbrace{c(\mathbf{x})(\kappa + V_0)|\nabla\phi|}_{\text{Gradient+Curvature-Forces}} + \underbrace{(\nabla c.\nabla\phi)}_{\text{Image-Force}} \right]. \tag{22}$$

If $[\phi^*(t) - \phi(t)]$ represented the optimized shape information at time t, then Leventon *et al.*added this term to the above equation to yield the final evolution equation in the level set framework as

$$\phi(t+1) = \phi(t) + \lambda_1 \left[\underbrace{c(\mathbf{x})(\kappa + V_0)|\nabla\phi|}_{\text{Gradient+Curvature-Forces}} + \underbrace{(\nabla c.\nabla\phi)}_{\text{Image-Force}} \right] + \underbrace{\lambda_2[\phi^*(t) - \phi(t)]}_{\text{Global-Shape-Force}}. \tag{23}$$

1) Design of the External Propagation Force Based on Global Shape Information: The key to the above model was the extraction of the shape information from the training data (called "global shape" information) and fusing with the local information (gradient and curvature) in the level set framework based on partial differential equations. If α and β represented shape and pose parameters, then the optimized ϕ^*_{MAP} would be given as the $\arg\max$ of $P(\phi^*|\phi, \nabla I)$. This model using Bayes' rule could be broken down as: $(P(\phi|\alpha, \beta)P(\nabla I|\alpha, \beta, \phi)P(\alpha)P(\beta))/(P(\phi, \nabla I))$, where $P(\alpha)$ and $P(\beta)$ were shape and pose priors. To understand the computation of $P(\alpha)$, Leventon took n-curves, each sampled N times and each surface was represented by ϕ_i. Then, the training set $\tau = \{\phi_i, \ldots \phi_n\}$. This mean shape could be computed as $\mu = (1/n)\Sigma\phi_i$ and the mean offset map was $\hat{\phi}_i = (\phi_i - \mu)$. Each of this map is a column vector of a matrix $(N \times n)$. If r, c represents the rows and columns of the matrix M, then $M = [\phi_{r,c}]$, where the limits r and c were: $1 \leq r \leq N$ and $1 \leq c \leq n$. Next, this matrix M undergoes singular value decomposition (SVD) to decompose to $U\Sigma V^T$. Taking k-principal components, that is k-rows and k-columns, gave the new matrix Σ. Thus the shape coefficients α were computed as: $\alpha = U_k^T(\phi - \mu)$. Using the Gaussian distribution, the priors shape model could be computed as

$$P(\alpha) = \frac{1}{\sqrt{(2\pi)^k|\Sigma|}} \exp\left(\frac{1}{2}\alpha^t\Sigma^{-1}\alpha\right). \tag{24}$$

This equation was used in the computation of optimized ϕ^*. The pose prior was from the uniform distribution.

Pros and Cons of Shape Information Fused in Geometric Boundary/Surface: The major advantages of this system were: 1) Robustness and successful capture of topology based on the Bayesian shape information. 2) Shape and pose parameters converged on the shape to be segmented. The major disadvantages of such a system were: 1) The time taken for such a system was six minutes (for vertebral segmentation), which was relatively very long for spinal navigation real-time applications. 2) The system would need training data sets which had to be collected off-line. 3) This paper did not show results on cortical segmentation which had deep convolutions, large twists and bends. 4) The performance of systems which had coefficients estimated from training data off-line and application of these estimated coefficients on-line was dependent upon training data and test data sets. The above system was like a first layer of a neural network (see Suri *et al.* [119]) where the performance was governed by shapes of training data and tuning parameters of the Gaussian model (see Lee *et al.* [120]).

E. Comparison Between Different Kinds of Regularizers

Having discussed four different kinds of regularizers (or design of propagating forces), this sub-section presents the comparison between them on the following points:

1) *Internal Versus External Propagating Force*: Primarily all of the regularizers design the propagating force and drive the speed term. Suri *et al.*'s technique designs the propagation force internal to the level set, while Leventon's technique designs the propagation force externally. The internal propagation force is accurate and robust since it directly acts on the speed function compared to the external propagation force. However, the internal propagation force is more sensitive to the overall system since these forces are computed directly based on region-based strategy and acted directly on speed functions.

2) *Common to All Techniques:* Suri's method uses fuzzy clustering, Zeng's method uses the constrained Bayesian approach, Barillot's technique uses plain Bayesian classification, and Leventon's technique uses the global shape-based information using Eigen analysis based on SVD. All of these techniques had one objective in common, that is, they were after the extraction of the shape to be segmented by fusion of the region-based strategy in the level set framework.

3) *Timings:* It is difficult to compare the speed since all of these four techniques do segmentation of different organs and volumes, and it also depended on the initial placement of the contour/surface. Individually, the claims of each of these techniques had the following timings: 1) Suri's 2-D GM/WM segmentation techniques took less than a minute per image. 2) Zeng's 3-D technique took around one hour for cortical segmentation. 3) Barillot's 3-D technique took around two hours for cortical segmentation. 4) Leventon's 3-D technique took six minutes for the complete vertebrae.

4) *User Interaction:* Suri's technique was automatic except for the placement of the initial contour. Zeng's method did initialization of sphere sets in white matter, which was at a minimum. Barillot's technique also involved minimal interaction. Leventon's technique used an off-line method for tracing the boundaries of shapes which was needed for training data sets. This was time consuming.

5) *Number of Parameters and Adaptability Toward Step Size:* The number of parameters used in Suri's technique was at a minimum for a particular tissue type for the MR image (e.g., T_1, T_2 or PD). The fuzzy clustering had two parameters, the error threshold and the number of iterations. The technique was not self-adaptive as far as the step sizes went. It was kept constant at unity. Zeng's method used a minimum number of parameters and was also not adaptive; however, the constrained force generation was dynamic. Barillot's method had also a minimum number of parameters but was self-adaptive. Leventon's method was not self-adaptive and used a greater number of parameters compared to the other techniques.

6) *Stability of the Method:* This factor depended upon a ratio, the Courant number. (See Section V-B.) No discussion was given about the CFL number by Suri *et al.*Barillot did discuss stability issues in which they talked about the dynamic nature of the CFL number that automatically changed to adjust for any instabilities.

V. Numerical Methodologies for Solving Level Set Functions

The relationship between conservation laws and the evolution of curves was introduced in the classic paper by Osher and Sethian [67]. This paper presented a new formulation for curve evolution by considering the evolution of a higher dimensional function in which the curve was embedded as a "level set." This was a stable and efficient numerical scheme (for the nonconvex Hamiltonian numerical scheme, readers are referred to Osher and Shu [106]).

This section has three parts: 1) Part one (Section V-A) is the derivation of the finite difference equation in terms of level sets using the Hamilton–Jacobi (HJ) and hyperbolic conservation law; 2) Part two (Section V-B) is on the ratio $\Delta t/\Delta x$, the so-called CFL number[17]; and 3) Part three (Section V-C) consists of the application of the numerical scheme using finite difference for cortical segmentation.

A. Hamilton–Jacobi Equation and Hyperbolic Conservation Law

Here, the numerical approximation of the Hamilton–Jacobi formulation of the level set function will be briefly derived. To start with, the hyperbolic conservation law stated that "the rate of change of the total amount of substance contained in a fixed domain G is equal to the flux of that substance across the boundary of G." If v was the density of the substance and f the flux, then the conservation law was mathematically given as: $(d/dt)\int_G v\,dx = -\int_{\partial G}\langle f, n\rangle\,dS$, where n was the outward normal to G, dS is the surface element of ∂G. Using vector calculus, the differential conservation law was: $v_t + \nabla.f = 0$. The HJ equation in $\mathcal{R}^d$ had the form: $\phi_t + H(\phi_{x1} \ldots \phi_{xd})$ and in 1-D, the HJ equation became the conservation law, and as a result, the methodologies used for solving the conservation law were used for solving the HJ equation. A finite difference method was in the conservation form if it could be written as

$$\frac{v_j^{n+1} - v_j^n}{\Delta t} = -\left(\frac{c_{j+1/2}^n - c_{j-1/2}^n}{\Delta x}\right) \tag{25}$$

where c was the potential field or the numerical flux, which was Lipschitz and consistent.[18] Thus using the relationship between the level set function, the HJ equation and the conservation law, we have: $\phi(x,t) = \int_{\infty}^{x} v(\hat{x}, t)\,d\hat{x}$. By integration over the monotone numerical scheme and shifting from $j+1/2$ to j, the HJ formulation was given as: $\phi_j^{n+1} = \phi_j^n - \Delta t\, c(D_-\phi_j^n, D_+\phi_j^n)$, where $c(D_-\phi_j^n, D_+\phi_j^n) = h[(\mathbf{min}(v_j^n, 0))^2 + (\mathbf{max}(v_j^n, 0))^2]$.[19] This equation will be used in the segmentation example in Section V-C, but first, the ratio $\Delta t/\Delta x$, the so-called CFL number, will be discussed.

B. CFL Number

For the stability of the numerical scheme, it was observed by Courant *et al.* [107] that a necessary stability condition for any numerical scheme was that the domain of dependence (DoD) of each point in the *domain of numerical scheme* should include the DoD of the partial differential equation itself. This condition was necessary for the stability of the numerical scheme. The ratio $\Delta t/\Delta x$ under the limit $\Delta x \to 0$ and $\Delta t \to 0$ is the CFL number, or called the Courant number. This CFL number was determined by the maximal possible flow of information. This flow of lines of information depended upon the type of the data and was thus called as "characteristics of the PDE." If these "characteristics" collide, then "shocks" occur. Interested readers can see the work by Kimia *et al.* [84] on shocks. Recently, Goldenberg *et al.* [108] fused the AOS[20] scheme in level sets for numerical stability. The original AOS model was presented by Perona–Malik [109] for nonlinear diffusion in image processing. Interested readers can explore the AOS model and its fusion in level sets by Goldenberg.

C. A Segmentation Example Using a Finite Difference Method

Here, speed control functions and their integration in terms of the level set function ϕ to estimate the ϕ over time are presented. The time step restrictions for solving the partial differential equation will not be discussed here (the reader can refer to the work by Osher and Sethian *et al.* [67] and the recent work by Barillot *et al.* [103]). Using the finite difference method (see also Sethian [71] and Rouy *et al.* [76]), the level set (17) was given in terms of time n as (for details, see Suri *et al.* [55] and [56])

$$\phi_{x,y}^{n+1} = \phi_{x,y}^n - \Delta t\{V_{reg}(x,y) + V_{\mathrm{grad}}(x,y) - V_{cur}(x,y)\} \tag{26}$$

where

$\phi_{x,y}^n$ and $\phi_{x,y}^{n+1}$ were level set functions at pixel location (x, y) at times n and $n+1$;

[17]Courant number, named after the author Courant *et al.* [107]

[18]Numerical flux becomes continuous flux, i.e., $c(v, \ldots, v) = H(v)$.

[19]Note, D_- and D_+ are the backward and forward difference operator.

[20]Additive operator splitting.

Δt	was the time difference;
$V_{reg}(x,y)$, $V_{\text{grad}}(x,y)$, and $V_{cur}(x,y)$	were the regional, gradient, and curvature speed terms, respectively.

Now, these terms are presented as under: 1) The regional speed term expressed in terms of the level set function (ϕ) was given as: $V_{reg}(x, y) = \mathbf{max}(V_p(x, y), 0)\nabla^+ + \mathbf{min}(V_p(x, y), 0)\nabla^-$, where terms $V_p(x, y)$, ∇^+ and ∇^- were given as: $V_p(x, y) = \omega_R/(\gamma R_{ind}(x, y))$, $R_{ind} = 1-2u(x, y)$, $\nabla^- = [\nabla_x^- + \nabla_y^-]^{1/2}$ and $\nabla^+ = [\nabla_x^+ + \nabla_y^+]^{1/2}$

$$\begin{cases} \nabla_x^+ = [\mathbf{max}(D^{-x}(x, y), 0))^2 + \mathbf{min}(D^{+x}(x, y), 0))^2] \\ \nabla_y^- = [\mathbf{max}(D^{-y}(x, y), 0))^2 + \mathbf{min}(D^{+y}(x, y), 0))^2] \end{cases} \tag{27}$$

where $u(x, y)$ took a value between zero and one. This could be coming from, say, a fuzzy membership function or any other clustering technique. R_{ind} was the region indicator function that was in the range between -1 to $+1$. 2) The gradient speed term, so-called the edge strength of the object boundaries, was expressed in terms of the level set function (ϕ) as the x and y components of the gradient speed as: $V_{\text{grad}}(x, y) = V_{\text{grad}x}(x, y) + V_{\text{grad}y}(x, y)$, where

$$\begin{cases} V_{\text{grad}x}(x, y) = \mathbf{max}(p^n(x, y), 0)D^{-x}(x, y) \\ \qquad\qquad +\mathbf{min}(q^n(x, y), 0)D^{+x}(x, y) \\ V_{\text{grad}y}(x, y) = \mathbf{max}(q^n(x, y), 0)D^{-y}(x, y) \\ \qquad\qquad +\mathbf{min}(q^n(x, y), 0)D^{+y}(x, y) \\ p^n(x, y) = \nabla_x(w_e\nabla(G_\sigma * I)) \text{ and} \\ q^n(x, y) = \nabla_y(w_e\nabla(G_\sigma * I)) \end{cases} \tag{28}$$

where w_e was the weight of the edge and was also a fixed constant. $p^n(x, y)$ and $q^n(x, y)$ were defined as the x and y components of the gradient strength at a pixel location (x, y). Note that the regional and edge speed terms depended upon the forward and backward difference operator which was defined in terms of the level set function ϕ defined as

$$\begin{cases} D^{-x}(x, y) = \dfrac{(\phi(x,y) - \phi(x-1,y))}{\Delta x} \text{ and} \\ D^{+x}(x, y) = \dfrac{(\phi(x+1,y) - \phi(x,y))}{\Delta x} \\ D^{-y}(x, y) = \dfrac{(\phi(x,y) - \phi(x,y-1))}{\Delta y} \text{ and} \\ D^{+y}(x, y) = \dfrac{(\phi(x,y+1) - \phi(x,y))}{\Delta y} \end{cases} \tag{29}$$

where $\phi(x, y)$, $\phi(x-1, y)$, $\phi(x+1, y)$, $\phi(x, y-1)$, $\phi(x, y+1)$ were the level set functions at pixel locations (x, y), $(x-1, y)$, $(x+1, y)$, $(x, y-1)$, $(x, y+1)$, being the four neighbors of (x, y). **3)** The curvature speed term expressed in terms of the level set function (ϕ) was given as: $V_{cur}(x, y) = \epsilon\kappa^n(x, y)[(D^{0x}(x, y))^2 + ((D^{0y}(x, y))^2]^{1/2}$, where ϵ was a fixed constant, $\kappa^n(x, y)$ was the curvature at a pixel location (x, y) at nth iteration as: $\kappa^n(x, y) = (\phi_{xx}^2\phi_y^2 - \phi_x^2\phi_y^2\phi_{xy}^2 + \phi_{yy}^2\phi_x^2)/((\phi_x^2 + \phi_y^2)^{3/2})$ and $D^{0x}(x, y)$ and $D^{0y}(x, y)$ were defined as

$$D^{0x}(x, y) = \frac{(\phi(x+1, y) - \phi(x-1, y))}{2\Delta x}$$

and

$$D^{0y}(x, y) = \frac{(\phi(x, y+1) - \phi(x, y-1))}{2\Delta y}. \tag{30}$$

Thus, to numerically solve (26), all that was needed was: 1) the gradient speed values (p, q); 2) the curvature speed κ at pixel location (x, y); and 3) the membership function $u(x, y)$ for a particular class K. In the next section, how these speeds control mathematical functions will be discussed and how they are used to compute the field flow (level set function, ϕ) in the "narrow band" using the "fast marching method," also called the "optimization technique."

VI. Optimization and Quantification Techniques Used in Conjunction With Level Sets: Fast Marching, Narrow-Band, Adaptive Algorithms, and Geometric Shape Quantification

The level set method could be computatively very expensive as the dimensionality of the surface increases. If d is the dimension of the surface, and $n = 1/\delta$ where δ is the length scale of the computational resolution, then the cost of tracking the surface can be reasonably expected to be of the order $O(n^\delta)$ per time step. There are two ways by which the speed can be improved. One way is by running the level set implementation in the narrow band (see Malladi *et al.* [77]) and the second is by using the adaptive mesh technique (see Milne *et al.* [116]). These will be discussed in this section. The algorithms in 2-D will be discussed, but it is straightforward to convert it into 3-D.

A. Fast Marching Method

The fast marching method (FMM) was used to solve the Eikonal Equation (see Adalsteinsson *et al.* [110]–[112], [123]), or a level set evolution with speed where the sign did not change. Its main usage was to compute the signed distance transform from a given curve (say, one with speed $= 1$). This signed distance function was the level set function that was used in the narrow band algorithm. The FMM can also be used for a simple active contour model if the contour only moved either inward (pressure force in terms of parametric snakes) or outward (balloon force in terms of parametric snakes). The FMM algorithm consisted of three major stages: 1) initialization stage; 2) tagging stage; and 3) marching stage. A discussion on these follows next.

1) *Initialization Stage*: If the curve cuts the grid points exactly, this means that the curve passed through the intersection of the horizontal and vertical grid lines. If the curve did not pass through the grid points, then it was necessary to find where the curve intersected the grid lines using the simple method recently developed by Adalsteinsson *et al.* [111]. The method consisted of checking

the neighbors (E, W, N, S) of a given central pixel and finding 16 different combinations where the given contour could intersect the grid. Since the central pixel could be inside or outside, there were 16 positive combinations and 16 negative combinations. At the end of this process, the distances of all the grid points were noted which were closest to the given curve.

2) *Tagging Stage*: Here, three sets of grid points were created: *accepted set*, *trial set* and *far set*. The *accepted set* were those points which fell on the given curve. All these points obviously had a distance of zero. Those points were tagged as ACCEPTED. If the curve did not pass through the grid points, then those points were points of the initialization stage and were tagged as ACCEPTED. The *trial set* included all points that were nearest neighbors to the point in the *accepted set*. Those were tagged as TRIAL. Then their distance values were computed by solving the Eikonal equation (5). Those points and their distances were put on the heap. The *far set* were grid points which were neither tagged as ACCEPTED nor TRIAL. Those were tagged as FAR. They did not affect the distance computation of trial grid points. These grid points were not put onto the heap.
3) *Marching Stage:*
    a) Here, the grid point (say, P) was popped from the top of the heap. It should have the smallest distance value among all grid points in the heap. This point was tagged as ACCEPTED so that its value would not change anymore. Heap sort methodology was used for bubbling the least distance value on the heap.
    b) Four nearest neighbors of the popped point P were found. If its tag was ACCEPTED, nothing was done; otherwise, the distance was recomputed by solving the Eikonal equation (5). If it was FAR, it was relabled as TRIAL and was put on the heap. If it is already labeled as TRIAL, its value was updated in the heap. This prevented the same point from appearing twice in the heap.
    c) Go back to step 3a) until there were no more points in the heap, i.e., all points had been tagged as ACCEPTED.

Note that the above method was an exhaustive search like the greedy algorithm discussed by Suri *et al.* [92]. The superiority of this method was evidenced by the fact that every visited grid point was visited no more than four times. The crux of the speed was due to the sorting algorithm. Suri *et al.* used the back pointer method at the grid or pixel location (x, y), similar to the approach taken by Sethian *et al.* [113], [114].

B. A Note on the Heap Sorting Algorithm

Heap sorting based on the back pointer method was first applied by Sethian/Malladi in their work (see Malladi *et al.* [49]). Since then, almost all researchers have used this technique in their implementations. The heap sorting algorithm was basically used to select the smallest value (see Sedwick *et al.* [115]). Briefly, a heap can be viewed as a tree or a corresponding ordered array. A binary heap had the property that the value at a given "child" position $\mathrm{int}(i)$ was always larger than or equal to the value at its "parent" position $(\mathrm{int}(i/2))$. The minimum travel time in the heap was stored at the top of the heap. Arranging the tentative travel time array onto a heap effectively identified and selected the minimum travel time in the array. The minimum travel time on the heap identified a corresponding minimum travel time grid point. Values could be added or removed from the heap. Adding or removing a value to/from the heap included rearranging the array so that it satisfied the heap condition ("heapifying the array"). Heapifying an array was achieved by recursively exchanging the positions of any parent–child pair violating the heap property until the heap property was satisfied across the heap. Adding or removing a value from a heap generally has a computational cost of order $\mathcal{O}(\log N)$, where N was the number of heap elements.

C. Narrow-Band Method

Malladi *et al.* [77] was one of the beginners who first applied the narrow banding scheme for medical image segmentation. Almost all the recent applications using level sets have used narrow banding in their implementations. Below are the steps that were followed for optimization of the level set function ϕ using narrow banding. The level set function computation was implemented in the narrow band, given the speed functions.

1) *Narrow-Band and Land Mine Construction*
    Here, a narrow band was constructed around the given curve where the absolute distance value was less than half the width of the narrow band. These grid points were put onto the list. Now some points in the narrow band were tagged as land mines. They were the grid points whose absolute distance value was less than $W/2$ and greater than $((W/2) - \Delta_l)$, where W was the band-width and Δ_l was the width of the land mine points. Note that the formation of the narrow band was equivalent to saying that the first external iteration or a new tube had been formed.
2) *Internal Iteration for Computing the Field Flow* (ϕ)
    This step evolved the active contour inside the narrow band until the land mine sign changed. For all the iterations, the level set function was updated by solving the level set equation (26). Now the land mine sign of its ϕ was checked. If the sign was changed, the system was reinitialized, otherwise the loop was continued.
3) *Re-Initialization [Zero Level Curve (ZLC) and Signed Distance Transform Computation]*
    This step consisted of two parts: 1) Determination of the *zero level curve* given the field flow ϕ. 2) Given the *zero level curve*, estimation was done of the signed distance transform (SDT). Part 1) is also called isocontour extraction since the front in the field flow is estimated which had a value of zero. The modified version of the Adalsteinsson *et al.* [111] algorithm was used for estimating the ZLC, however the signs of the field flow were needed. In part 2), the fast marching method was run

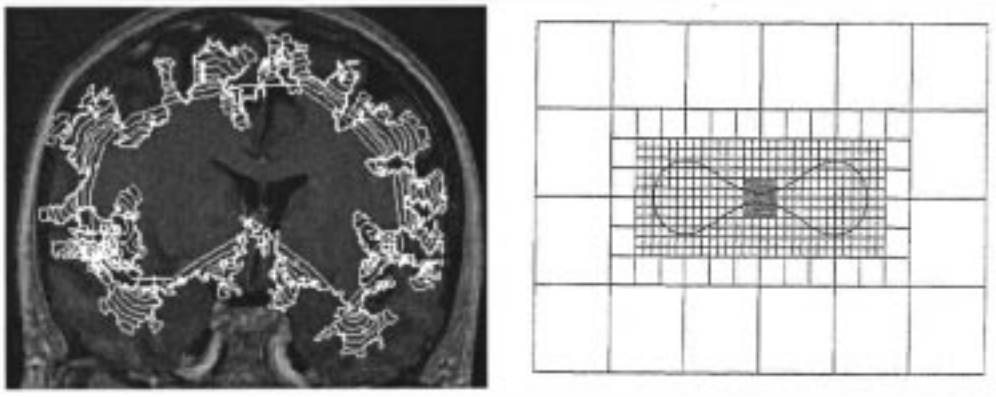

(a) (b)

Fig. 5. (a) Ripples formed during the growth evolution of *zero level curves*. Also seen is the large capture range of the segmentation scheme along with the shape change as per the topology. This figure shows superimposition of 6 *zero level set* curves (MR Data Set: Courtesy of Marconi Medical Systems, Inc.). (b) Adaptive mesh refinement. Reprinted with permission of R.B. Milne, Lawrence Berkeley National Laboratory, Berkeley, CA, LBNL-39216, p. 33, 1995.

to estimate the signed distance transform. The signed-distance-function was computed for all the points in the computational domain. At the end of step 3), the algorithm moved to step 1) and the next external iteration was started.

At the end of the process, a new *zero level curve* was estimated which represented the final object boundary. Note, this technique was used for all the global information integrated into the system.

D. A Note on Adaptive Level Sets Versus Narrow Banding

Adaptive level sets were attempted by Milne [116] while working toward the Ph.D. degree. In this method, the resolution of the grid was changed during the marching stage. Fig. 5 shows an example where the mesh resolution changed for the high curvature zones. This scheme had three major benefits: 1) The algorithm does not need to be re-initialized. **2**) The computational domain was extended beyond the surface of interest without the incurrence of a performance penalty. Thus the boundary conditions were not a serious threat to the stable solution. **3**) Adaptive level sets allowed for a nonuniform resolution of the surface itself. This meant one can selectively redistribute the density of information across the surface. As a result, one could match itself to the small scale features of the surface. Thus adaptive level sets are more powerful than plain narrow band level set methods. Even though adaptive level sets had done well compared to narrow band methods, the application of adaptive level sets in high curvature areas is not very stable. If the interface changed from coarse to fine, then stability issues of the propagating fronts are in question (see Berger *et al.* [94], [95]).

VII. Merits, Demerits, the Future and Conclusions of 2-D and 3-D Level Sets in Medical Imagery

A. Advantages of Level Sets

Level set formulation offers a large number of advantages that are as follows: 1) *Capture Range*: The greatest advantage of this technique is that this algorithm increases the capture range of the field flow and thereby increases the robustness of the initial contour placement. 2) *Effect of Local Noise*: When the regional information is integrated into the system, then the local noise or edge will not distract the growth process. This technique is nonlocal and thus the local noise cannot distract the final placement of the contour or the diffusion growth process. 3) *No Need of Elasticity Coefficients*: The technique is not controlled by elasticity coefficients, unlike parametric contour methods. There is no need to fit tangents to the curves and compute normals at each vertex. In this system, the normals are embedded in the system using the divergence of the field flow. This technique has an ability to model incremental deformations in shape. 4) *Suitability for Medical Image Segmentation*: This technique is very suitable for medical organ segmentation since it can handle any of the cavities, concavities, convolutedness, splitting or merging. 5) *Finding the Global Minima*: There is no problem finding the local minima or global minima, unlike optimization techniques of parametric snakes. 6) *Normal Computation*: This technique is less prone to the normal computational error which is very easily incorporated in classical balloon force snakes for segmentation. 7) *Automaticity*: It is very easy to extend this model from semi-automatic to completely automatic because the region is determined on the basis of prior information. 8) *Integration of Regional Statistics*: This technique is based on the propagation of curves (just like the propagation of ripples in the tank or propagation of the fire flames) utilizing the region statistics. 9) *Flexible Topology*: This method adjusts to the topological changes of the given shape. Diffusion propagation methods handle a very natural framework for handling the topological changes (joining and breaking of the curves). 10) *Wide Applications*: This technique can be applied to unimodal, bimodal, and multimodal imagery, which means it can have multiple gray level values in it. These methods have a wide range of applications in 3-D surface modeling. 11) *Speed of the System*: This technique implements the fast marching method in the narrow band for solving the Eikonal Equation for computing signed distances. 12) *Extension*: The technique is an easy extension from 2-D to 3-D. 13) *Incorporation of Regularizing Terms*: This can easily incorporate other features for controlling the speed of the curve. This is done by adding

an extra term to the region, gradient and curvature speed terms. 14) *Handling Corners*: The system takes care of the corners easily unlike parametric curves, where it needs special handling at corners of the boundary. 15) *Resolution Changes*: The technique is extendable to multi-scale resolutions, which means that at lower resolutions, one can compute regional segmentations. These segmented results can then be used for higher resolutions. 16) *Multi-Phase Processing*: This technique is extendable to multiphase, which means that if there are multiple level set functions, then they automatically merge and split during the course of the segmentation process. 17) *Surface Tracking*: Tracking surfaces are implemented using level sets very smoothly. 18) *Quantification of 3-D Structures*: Computation of geometrical computations is done in a natural way, for example, one can compute the curvature of 3-D surfaces directly while performing normal computations. 19) *Integration of Regularization Terms*: Allows easy integration of vision models for shape recovery such as in fuzzy clustering, Gibbs model, Markov Random Fields and Bayesian models (see Paragios *et al.* [29]). This makes the system very powerful, robust and accurate for medical shape recovery. 20) *Concise Descriptions*: One can give concise descriptions of differential structures using level set methods. This is because of background mesh resolution controls. 21) *Hierarchical Representations*: Level set offers a natural scale space for hierarchical representations. 22) *Reparameterization*: There is no need for reparameterization for curve/surface estimation during the propagation, unlike in the classical snakes model.

B. Disadvantages of Level Sets

Even though level sets have dominated several fields of imaging science, these front propagation algorithms have certain drawbacks. They are as follows: 1) *Initial Placement of the Contour*: One of the major drawbacks of parametric active contours was its initial placement. It does not have either enough capture range or enough power to grab the topology of shapes. Both of these drawbacks were removed by level sets provided the initial contour was placed *symmetrically* with respect to the boundaries of interest. This ensures that level sets reached object boundaries almost at the same time. On the contrary, if the initial contour is much closer to the first portion of the object boundary compared to the second portion, then the evolving contour crosses over the first portion of the object boundary. This is because the stop does not turn out to be zero. One of the controlling factors for the stop function is the gradient of the image. The relationship of the stop function to the gradient is its inverse, and also depends upon the index power m in the ratio $1/(1+|\nabla G_\sigma * I(x, y)|^m)$. For stopping the propagation, the denominator should be large, which means image forces due to the gradient should be high. This means index m should be high. In other words, if m is high, then the gradient is high, which means weak boundaries are not detected well and will be easily crossed over by the evolving curve. If m is low (low threshold), then the level set will stop at noisy or at isolated edges. 2) *Embedding of the Object*: If some objects (say, inner objects) are embedded in another object (the outer object), then the level set will not capture all objects of interest. This is especially true if embedded objects are asymmetrically situated. Under such conditions, one needs multiple initializations of active contours. This means only one active contour can be used per object. 3) *Gaps in Boundaries*: This is one of the serious drawbacks of the level set method and has been pointed out by Sidiqqui and Kimia. Due to gaps in the object, the evolving contour simply leaks through gaps. As a result, objects represented by incomplete contours are not captured correctly and fully. This is especially prominent in realistic images, such as in ultrasound and multi-class MR and CT images. 4) *Problems Due to Shocks*: Shocks are the most common problem in level sets. Kimia and co-workers [84]–[86] developed such a framework by representing shape as the set of singularities (so-called shocks) that arise in a rich space of shape deformations as classified into four types: 1) first-order shocks are orientation discontinuities (corners) and arise from protrusions and indentations; 2) second-order shocks are formed when a shape breaks into two parts during a deformation; 3) third-order shocks represent bends; and 4) fourth-order shocks are seeds for each component of a shape. These shocks arise in level sets and can cause sometimes serious problems.

C. Conclusions and the Future on Level Sets

The class of differential geometry, also called level sets, has been shown to dominate medical imaging in a major way. There is still a need to understand how regularization terms can be integrated into level sets to improve medical segmentation schemes. Even though the application of level sets has gone well in fields of medical imaging, biomedicine, fluid mechanics, combustion, solidification, CAD/CAM, object tracking/image sequence analysis, and device fabrication, this is still far away from achieving stable 3-D and a standard segmentation technique in real-time. By standard, this means that which can segment the 3-D volume with a wide variation of pulse sequence parameters. In the near future will be seen the modeling of front propagation that takes into account physical constraints of the problem, for example, minimization of variation geodesic distances, rather than simple distance transforms. Also will be seen more incorporation of likelihood functions and adaptive fuzzy models to prevent leaking of curves/surfaces. A good example of the integration of low level processes into the evolution process would be given as: $\partial\phi/\partial t = L(x, y)(\beta_0 - \beta_1\kappa)|\nabla\phi|$, where $L(x, y) = 1 - \max(S_1, S_2, S_3, \ldots, S_n)$, where S_i is the low level process from edge detection, optical flow, stereo disparity, texture, etc. The better the $S(x, y)$, the more robust would be the level set segmentation process. It is also hoped that more papers in level sets will be seen where the segmentation step does require a reinitialization stage (see Zhao *et al.* [121] and Evans *et al.* [122]). It would also, however, be helpful if a faster triangulation algorithm can be incorporated for isosurface extraction in 3-D segmentation methods.

A massive effort has been seen by the computer vision community to integrate regularization terms to improve robustness and accuracy of 3-D segmentation techniques. How curve/surface propagation hypersurfaces based on differential geometry are used was shown for the segmentation of medical objects in 2-D and 3-D. Also shown in this paper is the relationship

between parametric deformable models and curve evolution framework; incorporation of clamping/stopping forces to improve the robustness of these topologically independent curves/surfaces; and finally, state-of-the-art 2-D and 3-D level set segmentation systems was presented for medical imagery. With time, more adaptive schemes will be seen buffered with knowledge-based methods to yield more efficient techniques for 2-D and 3-D segmentation.

ACKNOWLEDGMENT

The authors would like to thank J. Patrick and E. Keeler, both with Marconi Medical Systems, Inc., for their encouragements. Special thanks go also to Marconi Medical Systems, Inc., for their MR data sets. Thanks go also to the anonymous reviewers for their valuable suggestions.

REFERENCES

[1] J. S. Suri, S. K. Setarehdan, and S. Singh, Advanced Algorithmic Approaches to Medical Image Segmentation: State-of-the-Art Applications in Cardiology, Neurology, Mammography and Pathology, 1st ed. London, U.K.: Springer-Verlag, 2001, to be published.

[2] J. S. Suri, "Two dimensional fast MR brain segmentation using a region-based level set approach," Int. J. Eng. Medicine Biol., vol. 20, no. 4, July/Aug. 2001, to be published.

[3] D. L. Chopp, "Computing minimal surfaces via level set curvature flow," *J. Comput. Phys.*, vol. 106, no. 1, pp. 77–91, 1993.

[4] J. O. Lachaud and A. Montanvert, "Deformable meshes with automated topology changes for coarse-to-fine 3D surface extraction," *Medical Image Anal.*, vol. 3, no. 2, pp. 187–207, 1999.

[5] J. O. Lachaud and E. Bainville, "A discrete adaptative model following topological modifications of volumes," in *Proc. 4th Discrete Geometry for Computer Imagery (DGCI)*, Grenoble, France, 1994, pp. 183–194.

[6] J. O. Lachaud and A. Montanvert, "Continuous analogs of digital boundaries: A topological approach to iso-surfaces," *Graphical Models and Image Processing (GMIP)*, vol. 62, no. 3, pp. 129–164, 2000.

[7] R. Malgouyres and A. Lenoir, "Topology preservation within digital surfaces," *Graphical Models*, vol. 62, no. 2, pp. 71–84, 2000.

[8] T. Y. Kong and A. Rosenfeld, "Digital topology: Introduction and survey," *Comput. Vision, Graphics, Image Processing*, vol. 48, no. 3, pp. 357–393, 1989.

[9] M. Bertalmio, G. Sapiro, and G. Randall, "Region tracking on level-sets methods," *IEEE Trans. Med. Imaging*, vol. 18, pp. 448–451, May 1999.

[10] D. DeCarlo and J. Gallier, "Topological evolution of surfaces," *Graphics Interface*, pp. 194–203, 1996.

[11] S. Angenent, D. Chopp, and T. Ilmanen, "On the singularities of cones evolving by mean curvature," *Commun. Partial Differential Equations*, vol. 20, no. 11/12, pp. 1937–1958, 1995.

[12] D. L. Chopp, "Flow under curvature: Singularity formation, minimal surfaces and geodesics," *Experimental Math.*, vol. 2, no. 4, pp. 235–255, 1993.

[13] ——, "Numerical computation of self-similar solutions for mean curvature flow," *Experimental Math.*, vol. 3, no. 1, pp. 1–15, 1993.

[14] J. A. Sethian, "Numerical algorithms for propagating interfaces: Hamilton–Jacobi equations and conservation laws," *J. Differential Geometry*, vol. 31, no. 1, pp. 131–161, 1990.

[15] ——, "Curvature flow and entropy conditions applied to grid generation," *J. Comput. Phys.*, vol. 115, no. 1, pp. 440–454, 1994.

[16] W. Mulder, S. J. Osher, and J. A. Sethian, "Computing interface motion in compressible gas dynamics," *J. Comput. Phys.*, vol. 100, no. 1, pp. 209–228, 1992.

[17] J. A. Sethian, "Algorithms for tracking interfaces in CFD and material science," *Annu. Rev. Comput. Fluid Mechanics*, 1995.

[18] M. Sussman, P. Smereka, and S. J. Osher, "A level set method for computing solutions to incompressible two-phase flow," *J. Comput. Phys.*, vol. 114, no. 1, pp. 146–159, 1994.

[19] C. Rhee, L. Talbot, and J. A. Sethian, "Dynamical study of a premixed V-flame," *J. Fluid Mechanics*, vol. 300, pp. 87–115, 1995.

[20] J. A. Sethian and J. D. Strain, "Crystal growth and dentritic solidification," *J. Comput. Phys.*, vol. 98, no. 2, pp. 231–253, 1992.

[21] D. Adalsteinsson and J. A. Sethian, "A unified level set approach to etching, deposition and lithography I: Algorithms and two-dimensional simulations," *J. Comput. Phys.*, vol. 120, no. 1, pp. 128–144, 1995.

[22] R. T. Whitaker, "Algorithms for implicit deformable models," in *Int. Conf. Comput. Vision (ICCV)*, June 1995, pp. 822–827.

[23] ——, "A level-set approach to 3D reconstruction from range data," *Int. J. Comput. Vision (IJCV)*, vol. 29, no. 3, pp. 203–231, Oct. 1998.

[24] R. T. Whitaker and D. E. Breen, "Level-set models for the deformation of solid objects," in *Proc. Implicit Surfaces, Eurographics/Siggraph*, June 1998, pp. 19–35.

[25] A. R. Mansouri and J. Konrad, "Motion segmentation with level sets," in *Proc. IEEE Int. Conf. Image Processing (ICIP)*, vol. II, Oct. 1999, pp. 126–130.

[26] A. R. Mansouri, B. Sirivong, and J. Konrad, "Multiple motion segmentation with level sets," *Proc. SPIE Image Video Commun. Processing*, vol. 3974, pp. 584–595, Apr. 2000.

[27] A.-R. Mansouri and J. Konrad, "Minimum description length region tracking with level sets," *Proc. SPIE Image Video Commun. Processing*, vol. 3974, pp. 515–525, Jan. 2000.

[28] N. Paragios and R. Deriche, "Geodesic active contours and level sets for the detection and tracking of moving objects," *IEEE Trans. Pattern Anal. Machine Intell.*, vol. 22, no. 3, pp. 266–280, Mar. 2000.

[29] ——, "Coupled geodesic active regions for image segmentation: A level set approach," in *The Sixth European Conference on Computer Vision (ECCV)*, vol. II. Dublin, Ireland, June 26–July 1, 2000, pp. 224–240.

[30] P. Kornprobst, R. Deriche, and G. Aubert, "Image sequence analysis via partial differential equations," *J. Math. Imaging Vision*, vol. 11, no. 1, pp. 5–26, 1999.

[31] O. Faugeras and R. Keriven, "Variational principles, surface evolution, PDE's level set methods and the stereo problem," *IEEE Trans. Image Processing*, vol. 7, pp. 336–344, May 1998.

[32] R. Kimmel, K. Siddiqi, and B. Kimia, "Shape from shading: Level set propagation and viscosity solutions," *Int. J. Comput. Vision*, vol. 16, no. 2, pp. 107–133, 1995.

[33] R. Kimmel, "Tracking level sets by level sets: A method for solving the shape from shading problem," *Comput. Vision Image Understanding*, vol. 62, no. 2, pp. 47–58, 1995.

[34] R. Kimmel and A. M. Bruckstein, "Global shape from shading," *Comput. Vision Image Understanding*, vol. 62, no. 3, pp. 360–369, 1995.

[35] A. Arehart, L. Vincent, and B. B. Kimia, "Mathematical morphology: The Hamilton–Jacobi connection," in *Int. Conf. Comput. Vision (ICCV)*, 1993, pp. 215–219.

[36] F. Catte, F. Dibos, and G. Koepfler, "A morphological scheme for mean curvature motion and applications to anisotropic diffusion and motion of level sets," *SIAM J. Numer. Anal.*, vol. 32, no. 6, pp. 1895–1909, 1995.

[37] G. Sapiro, R. Kimmel, D. Shaked, B. B. Kimia, and A. M. Bruckstein, "Implementing continuous-scale morphology via curve evolution," *Pattern Recognition*, vol. 26, no. 9, pp. 1363–1372, 1997.

[38] N. Sochen, R. Kimmel, and R. Malladi, "A geometrical framework for low level vision," *IEEE Trans. Image Processing*, vol. 7, pp. 310–318, 1998.

[39] G. Sapiro, "Color snakes," *Comput. Vision Image Understanding (CVIU)*, vol. 68, no. 2, pp. 247–253, 1997.

[40] V. Caselles, R. Kimmel, G. Sapiro, and C. Sbert, "Three dimensional object modeling via minimal surfaces," in *Proc. European Conf. Comput. Vision (ECCV)*, 1996, pp. 97–106.

[41] ——, "Minimal surfaces: A geometric three dimensional segmentation approach," *Numer. Math.*, vol. 77, no. 4, pp. 423–451, 1997.

[42] D. L. Chopp, "Computing minimal surfaces via level set curvature flow," *J. Comput. Phys.*, vol. 106, no. 1, pp. 77–91, 1993.

[43] R. Kimmel, A. Amir, and A. M. Bruckstein, "Finding shortest paths on surfaces using level sets propagation," *IEEE Trans. Pattern Anal. Machine Intell.*, vol. 17, pp. 635–640, June 1995.

[44] R. Malladi, R. Kimmel, D. Adalsteinsson, G. Sapiro, V. Caselles, and J. A. Sethian, "A geometric approach to segmentation and analysis of 3-D medical images," in *Proc. IEEE/SIAM Workshop Math. Morphology Biomed. Image Anal.*, San Francisco, CA, June 1996, pp. 244–252.

[45] R. Malladi and J. A. Sethian, "Image processing via level set curvature flow," *Proc. Nat. Academy Sci.*, vol. 92, no. 15, pp. 7046–7050, 1995.

[46] ——, "Image processing: Flows under min/max curvature and mean curvature," *Graphics Models Image Processing*, vol. 58, no. 2, pp. 127–141, 1996.

[47] ——, "A unified approach to noise removal, image-enhancement and shape recovery," *IEEE Trans. Image Processing*, vol. 5, pp. 1554–1568, Nov. 1996.

[48] R. Malladi, J. A. Sethian, and B. A. Vemuri, "A fast level set based algorithm for topology independent shape modeling," *J. Math. Imaging Vision (Special Issue on Topology and Geometry in Computer Vision)*, vol. 6, no. 2 and 3, pp. 269–290, Apr. 1996.

[49] R. Malladi and J. A. Sethian, "A real-time algorithm for medical shape recovery," in *Proc. Int. Conf. Comput. Vision*, Mumbai, India, Jan. 1998, pp. 304–310.

[50] R. Malladi, J. A. Sethian, and B. C. Vemuri, "Evolutionary fronts for topology-independent shape modeling and recovery," *Proc. 3rd Europ. Conf. Comput. Vision*, vol. 800, pp. 3–13, 1994.

[51] A. Yezzi, S. Kichenassamy, A. Kumar, P. Olver, and A. Tannenbaum, "A geometric snake model for segmentation of medical imagery," *IEEE Trans. Med. Imag.*, vol. 16, pp. 199–209, 1997.

[52] J. Gomes and O. Faugeras, "Level sets and distance functions," in *Proc. 6th Europ. Conf. Comput. Vision (ECCV)*, 2000, pp. 588–602.

[53] J. S. Suri, "Fast WM/GM boundary segmentation from MR images using the relationship between parametric and geometric deformable models," in Advanced Algorithmic Approaches to Medical Image Segmentation: State-of-the-Art Applications in Cardiology, Neurology, Mammography and Pathology, 1st ed, Suri, Setarehdan, and Singh, Eds. London, U.K.: Springer-Verlag, 2001, ch. 8, to be published.

[54] X. Zeng, L. H. Staib, R. T. Schultz, and J. S. Duncan, "Segmentation and measurement of the cortex from 3-D MR images using coupled-surfaces propagation," *IEEE Trans. Med. Imag.*, vol. 18, pp. 927–937, Sept. 1999.

[55] J. S. Suri, "Leaking prevention in fast level sets using fuzzy models: An application in MR brain," in *Proc. Int. Conf. Inform. Technol. Biomedicine*, Nov. 2000, pp. 220–226.

[56] J. S. Suri, "White matter/gray matter boundary segmentation using geometric snakes: A fuzzy deformable model," in *Proc. Int. Conf. Applicat. Pattern Recognition*. ser. Lecture Notes in Computer Science, S. Singh, N. Murshed, and W. Kropatsch, Eds. Rio: Springer-Verlag, Mar. 11–14, 2001, pp. 331–338.

[57] J. S. Suri, S. Singh, and L. Reden, "Computer vision and pattern recognition techniques for 2-D and 3-D MR cerebral cortical segmentation: A state-of-the-art review," J. Pattern Anal. Applicat., vol. 4, no. 3, Sept. 2001, to be published.

[58] G. Hermosillo, O. Faugeras, and J. Gomes, "Unfolding the cerebral cortex using level set methods," in *Proc. 2nd Int. Conf. Scale-Space Theories Computer.*, ser. Lecture Notes in Computer Sci., 1999, vol. 1682, p. 58.

[59] A. Sarti, C. Ortiz, S. Lockett, and R. Malladi, "A unified geometric model for 3-D confocal image analysis in cytology," in *Int. Symp. Comput. Graphics, Image Processing Vision*, Rio de Janeiro, Brazil, Oct. 20–23, 1998, pp. 69–76.

[60] W. J. Niessen, B. M. ter Haar Romeny, and M. A. Viergever, "Geodesic deformable models for medical image analysis," *IEEE Trans. Med. Imag.*, vol. 17, pp. 634–641, Aug. 1998.

[61] J. A. Sethian, "A review of recent numerical algorithms for hypersurfaces moving with curvature dependent flows," *J. Differential Geometry*, vol. 31, pp. 131–161, 1989.

[62] ——, "Theory, algorithms and applications of level set methods for propagating interfaces," *Acta Numer.*, vol. 5, pp. 309–395, 1996.

[63] R. Kimmel, N. Kiryati, and A. M. Bruckstein, "Analyzing and synthesizing images by evolving curves with the Osher–Sethian method," *Int. J. Comput. Vision*, vol. 24, no. 1, pp. 37–55, 1997.

[64] J. S. Suri, "Computer vision, pattern recognition, and image processing in left ventricle segmentation: Last 50 years," *J. Pattern Anal. Applicat.*, vol. 3, pp. 209–242, 2000.

[65] D. Terzopoulous and K. Fleischer, "Deformable models," *Visual Comput.*, vol. 4, no. 6, pp. 306–331, Dec. 1988.

[66] W. Kass and D. Terzopolous, "Snakes: Active contour models," *Int. J. Comput. Vision*, vol. 1, no. 4, pp. 321–331, 1988.

[67] S. Osher and J. Sethian, "Fronts propagating with curvature-dependent speed: Algorithms based on Hamiltons–Jacobi formulations," *J. Comput. Phys.*, vol. 79, no. 1, pp. 12–49, 1988.

[68] J. A. Sethian, "An analysis of flame propagation," Ph.D. dissertation, Dept. Math., Univ. California, Berkeley, CA, 1982.

[69] J. S. Suri *et al.*, "Modeling segmentation via deformable regularizers, PDE level sets in still/motion imagery: A revisit," Int. J. Image Graphics, vol. 1, no. 4, Dec. 2001, submitted for publication.

[70] M. Grayson, "The heat equation shrinks embedded plane curves to round points," *J. Differential Geometry*, vol. 26, pp. 285–314, 1987.

[71] J. A. Sethian, *Level Set Methods and Fast Marching Methods: Evolving Interfaces in Computational Geometry, Fluid Mechanics, Computer Vision and Material Science*, 2nd ed. Cambridge, U.K.: Cambridge Univ. Press, 1999.

[72] S. Cao and S. Greenhalgh, "Finite-difference solution of the Eikonal equation using an efficient, first-arrival, wavefront tracking scheme," *Geophysics*, vol. 59, no. 4, pp. 632–643, April 1994.

[73] S. Chen, B. Merriman, S. Osher, and P. Smereka, "A simple level set method for solving Stefan problems," *J. Comput. Phys.*, vol. 135, no. 1, pp. 8–29, 1997.

[74] S. Kichenassamy, A. Kumar, P. Olver, A. Tannenbaum, and A. Yezzi, "Conformal curvatures flows: From phase transitions to active vision," *Arch. Rational Mech. Anal.*, vol. 134, no. 3, pp. 275–301, 1996.

[75] V. Caselles, F. Catte, T. Coll, and F. Dibos, "A geometric model for active contours," *Numer. Math.*, vol. 66, no. 1, pp. 1–31, 1993.

[76] E. Rouy and A. Tourin, "A viscosity solutions approach to shape-from-shading," *SIAM J. Numer. Anal.*, vol. 23, no. 3, pp. 867–884, 1992.

[77] R. Malladi, J. A. Sethian, and B. C. Vemuri, "Shape modeling with front propagation," *IEEE Trans. Pattern Anal. Machine Intell.*, vol. 17, pp. 158–175, Feb. 1995.

[78] R. Malladi and J. A. Sethian, "An $O(N \log N)$ algorithm for shape modeling," *Appl. Math., Proc. Nat. Academy Sci.*, vol. 93, no. 18, pp. 9389–9392, Sept. 1996.

[79] K. Siddiqui, Y. B. Lauriere, A. Tannenbaum, and S. W. Zucker, "Area and length minimizing flows for shape segmentation," *IEEE Trans. Image Processing*, vol. 7, pp. 433–443, 1998.

[80] K. Siddiqi, A. Tannenbaum, and S. W. Zucker, "Hyperbolic smoothing of shapes," in *Proc. 6th Int. Conf. Comput. Vision (ICCV)*, vol. 1, Bombay, India, 1998, pp. 215–221.

[81] L. M. Lorigo, O. Faugeras, W. E. L. Grimson, R. Keriven, R. Kikinis, and C.-F. Westin, "Co-dimension 2 geodesic active contours for MRA segmentation," in *Proc. 16th Int. Conf. Inform. Processing Medical Imaging*, ser. Lecture Notes in Computer Science Visegrad, Hungary, June/July 1999, vol. 1613, pp. 126–139.

[82] L. M. Lorigo, W. Grimson, L. Eric, O. Faugeras, R. Keriven, R. Kikinis, A. Nabavi, and C.-F. Westin, "Two geodesic active contours for the segmentation of tubular structures," in *Proc. Comput. Vision Pattern Recognition*, June 2000, pp. 444–451.

[83] J. S. Suri and R. Bernstien, "2-D and 3-D display of aneurysms from magnetic resonance angiographic data," in *Proc. 6th Int. Conf. Comput. Assisted Radiology*, 1992, pp. 666–672.

[84] B. B. Kimia, A. R. Tannenbaum, and S. W. Zucker, "Shapes, shocks and deformations, I: The components of shape and the reaction-diffusion space," *Int. J. Comput. Vision (IJCV)*, vol. 15, no. 3, pp. 189–224, 1995.

[85] K. Siddiqi, K. J. Tresness, and B. B. Kimia, "Parts of visual form: Ecological and psychophysical aspects," *Perception*, vol. 25, no. 4, pp. 399–424, 1996.

[86] P. Stoll, H. Tek, and B. B. Kimia, "Shocks from images: Propagation of orientation elements," in *Proc. Comput. Vision Pattern Recognition*, Puerto Rico, June 15–16, 1997, pp. 839–845.

[87] V. Caselles, R. Kimmel, and G. Shapiro, "Geodesic active contours," *Int. J. Comput. Vision*, vol. 22, no. 1, pp. 61–79, 1997.

[88] A. Yezzi, A. Tsai, and A. Willsky, "A statistical approach to snakes for bimodal and trimodal imagery," in *Proc. Int. Conf. Comput. Vision*, 1999, pp. 898–903.

[89] Y. Guo and B. Vemuri, "Hybrid geometric active models for shape recovery in medical images," in *Proc. Int. Conf. Inf. Proc. Med. Imaging*, 1999, pp. 112–125.

[90] .C. Xu, "On the relationship between the parametric and geometric active contours,", Baltimore, MD, Internal Tech. Rep., 1999.

[91] G. Aubert and L. Blanch-Féraud, "Some remarks on the equivalence between 2D and 3D classical snakes and geodesic active contours," *Int. J. Comput. Vision*, vol. 34, no. 1, pp. 19–28, 1999.

[92] J. S. Suri, R. M. Haralick, and F. H. Sheehan, "Greedy algorithm for error correction in automatically produced boundaries from low contrast ventriculograms," *Int. J. Pattern Applicat. Anal.*, vol. 1, no. 1, pp. 39–60, Jan. 2000.

[93] J. C. Bezdek and L. O. Hall, "Review of MR image segmentation techniques using pattern recognition," *Med. Phys.*, vol. 20, no. 4, pp. 1033–1048, Mar. 1993.

[94] M. Berger and P. Colella, "Local adaptive mesh refinement for shock hydrodynamics," *Math. Comput.*, vol. 45, no. 142, pp. 301–318, Oct. 1985.

[95] M. J. Berger, "Local adaptive mesh refinement," *J. Comput. Phys.*, vol. 82, no. 1, pp. 64–84, 1989.

[96] J. A. Sethian, "Curvature flow and entropy conditions applied to grid generation," *J. Comput. Phys.*, vol. 115, no. 2, pp. 440–454, 1994.

[97] A. J. Tababai and O. R. Mitchell, "Edge location to subpixel values in digital imagery," *IEEE Trans. Pattern Anal. Machine Intell.*, vol. PAMI-6, pp. 188–201, Mar. 1984.

[98] A. Huertas and G. Medioni, "Detection of intensity changes with subpixel accuracy using Laplacian–Gaussian masks," *IEEE Trans. Pattern Anal. Machine Intell.*, vol. PAMI-8, pp. 651–664, Sept. 1986.
[99] J. Gao, A. Kosaka, and A. C. Kak, "A deformable model for human organ extraction," in *Proc. IEEE Int. Conf. Image Processing (ICIP)*, vol. 3, Chicago, IL, Oct. 1998, pp. 323–327.
[100] X. Zeng, L. H. Staib, R. T. Schultz, and J. S. Duncan, "Segmentation and measurement of the cortex from 3-D MR images," *Med. Image Comput. Computer-Assisted Intervention*, pp. 519–530, 1998.
[101] W. M. Wells, III, W. E. L. Grimson, R. Kikinis, and F. A. Jolesz, "Adaptive segmentation of MRI data," *IEEE Trans. Med. Imag.*, vol. 15, pp. 429–442, Aug. 1992.
[102] W. E. Lorenson and H. Cline, "Marching cubes: A high resolution 3-D surface construction algorithm," in *Proc. ACM Comput. Graphics*, vol. 21, July 1987, pp. 163–169.
[103] C. Baillard, P. Hellier, and C. Barillot, "Segmentation of 3-D brain structures using level sets," IRISA, Rennes Cedex, France, Res. Rep. 1291, Jan. 2000.
[104] C. Baillard, C. Barillot, and P. Bouthemy, "Robust adaptive segmentation of 3-D medical images with level sets," IRISA, Rennes Cedex, France, Res. Rep. 1369, Nov. 2000.
[105] C. Baillard, P. Hellier, and C. Barillot, "Cooperation between level set techniques and dense 3d registration for the segmentation of brain structures," in *Int. Conf. Pattern Recognition*, vol. 1, Sept. 2000, pp. 991–994.
[106] S. Osher and C. W. Shu, "Higher-order essentially nonoscillatory schemes for Hamilton–Jacobi equations," *SIAM J. Numer. Anal.*, vol. 28, no. 4, pp. 907–922, 1991.
[107] R. Courant, K. O. Friedrichs, and H. Lewy, "On the partial difference equations of mathematical physics," *IBM J.*, vol. 11, pp. 215–235, 1967.
[108] R. Goldenberg, R. Kimmel, E. Rivlin, and M. Rudzsky, "Fast geodesic contours," in *Proc. Scale-Space Theories Comput. Vision (SSTCV)*, 1999, pp. 34–45.
[109] P. Perona and J. Malik, "Scale space and edge detection using anisotropic diffusion," *IEEE Trans. Pattern Anal. Machine Intell.*, vol. 12, no. 7, pp. 629–639, Apr. 1993.
[110] D. Adalsteinsson and J. A. Sethian, "A fast level set method for propagating interfaces," *J. Comput. Phys.*, vol. 118, no. 2, pp. 269–277, May 1995.
[111] ——, "The fast construction of extension velocities in level set methods," *J. Comput. Phys.*, vol. 148, no. 1, pp. 2–22, 1999.
[112] D. Adalsteinsson, R. Kimmel, R. Malladi, and J. A. Sethian, "Fast marching methods for computing the solutions to static Hamilton–Jacobi equations," Univ. California, Berkeley, CA, CPAM Rep. 667.
[113] J. A. Sethian, "A fast marching level set method for monotonically advancing fronts," *Proc. Nat. Academy Sci., Appl. Math.*, vol. 93, no. 4, pp. 1591–1595, Feb. 1996.
[114] ——, "Three-dimensional seismic imaging of complex velocity structures," US Patent: 6 018 499, Jan. 25, 2000.
[115] R. Sedgewick, *Algorithms in C, Fundamentals, Data Structures, Sorting, Searching*. Reading, MA: Addison-Wesley, 1998, vol. 1.
[116] R. B. Milne, "An adaptive level set method," Ph.D. dissertation, Dept. Math., Berkeley, CA, Dec. 1995.
[117] M. E. Leventon, W. Grimson, L. Eric, and O. Faugeras, "Statistical shape influence in geodesic active contours," *Proc. Comput. Vision Pattern Recognition (CVPR)*, vol. 1, pp. 316–323, June 2000.
[118] T. F. Cootes, C. J. Taylor, D. H. Cooper, and J. Graham, "Active shape models: Their training and applications," *Comput. Vision Image Understanding*, vol. 61, no. 1, pp. 38–59, Jan. 1995.
[119] J. S. Suri, R. M. Haralick, and F. H. Sheehan, "Automatic quadratic calibration for correction of pixel classifier boundaries to an accuracy of 2.5 mm: An application in X-ray heart imaging," in *Int. Conf. Pattern Recognition*, Brisbane, Australia, Aug. 17–20, 1998, pp. 30–33.
[120] C. K. Lee, "Automated boundary tracing using temporal information," Ph.D. dissertation, Department of Electrical Engineering, University of Washington, Seattle, WA, 1994.
[121] H. K. Zhao, T. Chan, B. Merriman, and S. Osher, "A variational level set approach to multiphase motion," *J. Comput. Phys.*, vol. 127, no. 1, pp. 179–195, 1996.
[122] L. C. Evans and J. Spruck, "Motion of level sets by mean curvature: Part I," *J. Differential Geometry*, vol. 33, no. 3, pp. 635–681, 1991.
[123] D. Adalsteinsson, R. Kimmel, R. Malladi, and J. A. Sethian, "Fast marching methods for computing the solutions to static Hamilton–Jacobi equations," SIAM J. Numer. Anal., Feb. 1996, submitted for publication.

Jasjit S. Suri (S'90–M'91–SM'00) was born in India. He received the Bachelor's degree in electronics and computer engineering from Maulana Azad College of Technology, Bhopal, India, the Master's degree in computer science from the University of Illinois, Chicago, with specialization in neuro imaging, and the Doctorate degree in electrical engineering from University of Washington, Seattle, with specialization in cardiac imaging.

He has been working in the field of computer engineering/sciences for more than 18 years and in the field of segmentation for more than a 12 years. He has published more than 80 publications in the area of cardiac, brain, abdomen CT, dental, ultrasound, and cytology imaging. Recently he published a book in the area of segmentation applied to cardiology, neurology, mammography, and pathology imaging. He has presented his research work at several international conferences in Europe, Australia, and the United States. He has also worked with IBM Scientific Center, Siemens Research Division, and as a Scientist at University of Wisconsin, Madison in MR angiography, CT, and Ultrasound, respectively. He was a faculty member at MACT, Bhopal, India where he taught Computer Architecture Design. Currently, he is a Staff Scientist at Philips Medical Systems, Inc., (previously known as Picker International), Cleveland, OH, where he has contributed in software design for image guided surgery systems for brain and orthopedics, MR breast imaging, and MR angiography, respectively. He holds several United States Patents. His major interests are imaging sciences, graphical interfaces, component object modeling for cancer treatments, and diagnostic systems designs.

Dr. Suri is on the review/editorial boards of several imaging science international journals, including *Journal of Real Time Imaging*, *Journal of Engineering Medicine and Biology*, *Journal of Computer Assisted Tomography*, *Journal of Pattern Analysis and Applications*, *Journal of Radiology*, IEEE TRANSACTIONS ON INFORMATION TECHNOLOGY AND BIOMEDICINE. He has also served as a board member of the program committee of "Image Processing of International Association of Science and Technology for Development (IASTED)," program committee of "IEEE Computerized-Based Medical Systems" hosted by National Institutes of Health, program committee of "International Conference on Visualization, Imaging and Image Processing" hosted by IASTED and has reviewed several peer reviewed international conferences/journal papers in the areas of medical imaging and mathematical imaging. He is a member of Sigma Xi Research Honor Society, Tau Beta Phi Research Honor Society, New York Academy of Sciences, SPIE, EMBS and ACM. He has received more than 45 scholarly and extracurricular awards during his career, including the Indian President's Gold Medal in 1980.

Kecheng Liu was born in China. He received the B.Sc. degree from the Department of Scientific Instruments, Zhejiang University, Hangzhou, China, the M.Sc. from the Department of Electrical Engineering, Swiss Federal Institute of Technology, Zurich, Switzerland, and the Ph.D. degree from The Institute of Biomedical Engineering and Information, Swiss Federal Institute of Technology, Zurich, Switzerland.

He was a faculty member at Zhejiang University. He is currently working for Philips Medical Systems, Inc., Cleveland, OH, as a senior scientist. He has been working in the area of biomedical engineering, particularly magnetic resonance imaging, for more than 14 years and has had several publications and patents in the area of functional studies, quantification and hemodynamic study of blood flow, cardiac, angiography, interventional applications and 3-D acquisition methodology. He has presented his research work at several known international conferences in Europe and United States. He has also worked with Instrumentarium Imaging Inc., Picker Nordstar, Inc. and the John Roberts Research Institute.

Dr. Liu holds a membership of International Society of Magnetic Resonance in Medicine (ISMRM). His major interests are in: 2-D and 3-D segmentation and registration, hemofluid dynamics, magnetic resonance methodology study for different imaging modalities.

Sameer Singh (M'98) was born in New Delhi, India, and received the Bachelor of Engineering degree with distinction in computer engineering from Birla Institute of Technology, India. He received the Master of Science degree in information technology for manufacturing from the University of Warwick, U.K., and the Ph.D. degree in speech and language analysis of stroke patients from the University of the West of England, U.K.

He is the Director of the Pattern Analysis and Neural Networks Group at Exeter University. His main research interests are in image processing, medical imaging, neural networks and pattern recognition.

Dr. Singh serves as the Editor-in-Chief of the *Pattern Analysis and Applications* journal by Springer, Editor-in-Chief of the Springer book series on "Advances in Pattern Recognition," Chairman of the British Computer Society Specialist group on Pattern Analysis and Robotics, Editorial Board member of Neural Computing and Applications journal, and Editorial Board member of the Perspectives in Neural Computing book series by Springer. He is a Fellow of the Royal Statistical Society, and a Member of BMVA-IAPR and the Institute of Electrical Engineers, U.K.

Swamy N. Laxminarayan (M'79–SM'94) has held several senior positions both in industry and academia. These have included serving as the Chief Information Officer at the National St. Louis University in Chicago, Director of the VocalTec Corporate University in New Jersey, Director of the Bay Networks Authorized Center, Director of the Pharmaceutical and Health Care Information Services at NextGen Internet, the premier Internet organization that spun off from the NSF sponsored John von Neuman National Supercomputer Center, Princeton, NJ, Program Director of Biomedical Computing at the University of Medicine and Dentistry in New Jersey and Director of Clinical Computing at the Montefiore Hospital and Medical Center in New York. He has also served as an Adjunct Professor of Biomedical Engineering at the New Jersey Institute of Technology, a Clinical Associate Professor of Health Informatics, Visiting Professor of Biomedical Engineering at the University of Brno in Czech Republic and an Honorary Professor of Health Sciences at Tsinghua University in China. As an educator, researcher, and technologist, he has been involved in biomedical engineering and information technology applications in medicine and health care for over 20 years and has published extensively in international journals, books and conferences. His expertise are in the areas of biomedical information technology, high-performance computing, digital signals and image processing and physiological systems analysis. He is the Founding Editor-in-Chief and an Editor Emeritus of the IEEE TRANSACTIONS ON INFORMATION TECHNOLOGY IN BIOMEDICINE. His contributions to the field have earned him numerous national and international awards. He is a Fellow of the American Institute of Medical and Biological Engineering, a recipient of the IEEE Third Millennium Medal and a recipient of the Purkynje award from the Czech Academy of Medical Societies. He can be reached at s.n.laxminarayan@ieee.org

Xiaolan Zeng (M'00) received the B.S. degree in electrical engineering from University of Science and Technology, China in 1995, and the Ph.D. degree in electrical engineering from Yale University, New Haven, CT, in 2000.

She currently works as a Staff Scientist at R2 Technology, Inc. Her research interests include medical image analysis, computer-assisted intervention, and computered-aided detection.

Laura Reden was born in Yonkers, NY. She received the B.S. degree in chemistry from The College of New Rochelle, New Rochelle, NY.

She has been working in the field of MRI for more than 20 years. She is currently working at Philips Medical Systems, Inc., Cleveland, Oh, as a Clinical Ttesting Specialist. In this position, she is involved with testing any new aspect for the MRI system, both in-house and in the field. She is active in attending seminars on topics such as fMRI, breast imaging, and advanced neurological techniques for areas such as brain attack. She has coauthored two journal articles and has applied for patents related to MRI.